Mon. Not. R. Astron. Soc. **369,** 1303–1320 (2006) doi:10.1111/j.1365-2966.2006.10374.x

SN 2004A: another Type II-P supernova with a red supergiant progenitor

M. A. Hendry,[1] S. J. Smartt,[2⋆] R. M. Crockett,[2] J. R. Maund,[3] A. Gal-Yam,[4]†
D.-S. Moon,[5] S. B. Cenko,[5] D. W. Fox,[4] R. P. Kudritzki,[6] C. R. Benn[7] and R. Østensen[7]

[1]*Institute of Astronomy, University of Cambridge, Madingley Road, Cambridge CB3 0HA*
[2]*Department of Physics and Astronomy, Queen's University Belfast, Belfast BT7 1NN*
[3]*Astronomy Department, University of Texas, 1 University Station, C1400, Austin, TX 78712, USA*
[4]*Department of Astronomy, MS 105-24, California Institute of Technology, Pasadena, CA 91125, USA*
[5]*Department of Physics and Space Radiation Laboratory, MS 220-47, California Institute of Technology, Pasadena, CA 91125, USA*
[6]*Institute for Astronomy, University of Hawaii, 2680 Woodlawn Drive, Honolulu, HI 96822, USA*
[7]*Isaac Newton Group, Apartado 321, E-38700 Santa Cruz de La Palma, Spain*

Accepted 2006 March 23. Received 2006 March 22; in original form 2005 November 24

ABSTRACT

We present a monitoring study of SN 2004A and probable discovery of a progenitor star in pre-explosion *Hubble Space Telescope* (*HST*) images. The photometric and spectroscopic monitoring of SN 2004A show that it was a normal Type II-P which was discovered in NGC 6207 about two weeks after explosion. We compare SN 2004A to the similar Type II-P SN 1999em and estimate an explosion epoch of 2004 January 6. We also calculate three new distances to NGC 6207 of $21.0 \pm 4.3, 21.4 \pm 3.5$ and 25.1 ± 1.7 Mpc. The former was calculated using the Standard Candle Method (SCM) for SNe II-P, and the latter two from the brightest supergiants method (BSM). We combine these three distances with existing kinematic distances, to derive a mean value of 20.3 ± 3.4 Mpc. Using this distance, we estimate that the ejected nickel mass in the explosion is $0.046^{+0.031}_{-0.017}\,M_{\odot}$. The progenitor of SN 2004A is identified in pre-explosion WFPC2 F814W images with a magnitude of $m_{\rm F814W} = 24.3 \pm 0.3$, but is below the detection limit of the F606W images. We show that this was likely a red supergiant (RSG) with a mass of $9^{+3}_{-2}\,M_{\odot}$. The object is detected at 4.7σ above the background noise. Even if this detection is spurious, the 5σ upper limit would give a robust upper mass limit of $12\,M_{\odot}$ for a RSG progenitor. These initial masses are very similar to those of two previously identified RSG progenitors of the Type II-P SNe 2004gd ($8^{+4}_{-2}\,M_{\odot}$) and 2005cs ($9^{+3}_{-2}\,M_{\odot}$).

Key words: stars: evolution – supernovae: general – supernovae: individual: SN 2004A – galaxies: distances and redshifts – galaxies: individual: NGC 6207.

1 INTRODUCTION

Supernovae (SNe) are associated with the deaths of stars, in particular core-collapse supernovae (CCSNe) are associated with the deaths of massive stars, which have initial masses greater than about $8\,M_{\odot}$. SNe are principally separated into two categories, those without hydrogen (Type I) and those with (Type II). Only Type Ia SNe are thought to be thermonuclear explosions, which arise from accreting white dwarfs in binary stellar systems. All the other subtypes are thought to be initiated by the core collapsing in massive stars. The type of SN that occurs depends on the massive star's evolutionary stage at the time of the explosion. The plateau subclass of Type II SNe (SNe II-P) are thought to arise from the explosions of red supergiants (RSGs), which have initial masses greater than 8–10 $M_{\odot}$ and have retained their hydrogen envelopes before core collapse (Chevalier 1976; Baron, Cooperstein & Kahana 1985; Heger et al. 2003; Eldridge & Tout 2004).

Until the discovery of the RSG that exploded as SN 2003gd (Van Dyk, Li & Filippenko 2003b; Smartt et al. 2004; Hendry et al. 2005), there had been no direct confirmation that SNe II-P did indeed arise from the explosions of RSGs. Before this detection, there had been only two other unambiguous detections of Type II progenitors, neither of which fitted the evolutionary scenario that is commonly accepted. These were the progenitors of the peculiar Type II-P SN 1987A, which was a blue supergiant (BSG, White & Malin 1987; Walborn et al. 1989), and the Type IIb SN 1993J that arose in a

⋆E-mail: S.Smartt@qub.ac.uk
†Hubble Fellow.

massive interacting binary system (Aldering, Humphreys & Richmond 1994; Van Dyk et al. 2002; Maund et al. 2004). The recent discovery of SN 2005cs (II-P) in M51, a galaxy with deep multicolour pre-explosion images from the *Hubble Space Telescope* (*HST*), led to the discovery of another RSG progenitor of a II-P (Maund, Smartt & Danziger 2005; Li et al. 2006). The estimated mass of the star was $M_{\rm MS} = 9^{+3}_{-2}\,{\rm M}_{\odot}$, similar to the mass ($M_{\rm MS} = 8^{+4}_{-2}\,{\rm M}_{\odot}$) for the progenitor of SN 2003gd (Van Dyk et al. 2003b; Smartt et al. 2004). A supergiant of mass $M_{\rm MS} = 15^{+5}_{-2}\,{\rm M}_{\odot}$ was found to be coincident with the Type II-P SN 2004et by Li et al. (2005), although it is likely not to have been as cool as an M-type supergiant, and the SN itself may be peculiar. There have been other extensive attempts to detect progenitors of nearby SNe on ground- and space-based archival images, for example, Maund & Smartt (2005); Smartt et al. (2003); Van Dyk, Li & Filippenko (2003a); Maíz-Apellániz et al. (2004), which have set upper mass limits mostly on II-P events. The low mass of the progenitors discovered and upper limits set has led to the suggestion that SNe II-P come only from RSGs with masses less than about $15\,{\rm M}_{\odot}$ (Maund 2005; Li et al. 2006).

SN 2004A is another example of a nearby SN II-P which has *HST* pre-explosion images, allowing the search for a progenitor star. SN 2004A was discovered by K. Itagaki of Teppo-cho, Yamagata, Japan on January 9.84 UT using a 0.28-m f/10 reflector. Itagaki confirmed his discovery on January 10.75 UT, with a location of RA $= 16^h43^m01.90^s$, Dec. $= +36^\circ50'12.5''$, around 22 arcsec west and 17 arcsec north of the centre of NGC 6207. Itagaki reported that no object was visible on his observations of 2003 December 27, which had a limiting magnitude of 18, or any of his observations prior to this date (Nakano et al. 2004). Itakagi's observations allow the explosion epoch to be fairly well constrained, suggesting that SN 2004A was discovered when it was quite young at less than 14 d after explosion. An optical spectrum was obtained by Kawakita et al. (2004) on January 11.8 and 11.9 UT, and showed a blue continuum with P-Cygni profiles of the Balmer lines, consistent with a Type II SN. The emission features were somewhat weak suggesting that the SN was indeed young, in line with Itagaki's observations. The expansion velocity, measured from the minima of the Balmer lines, was around $12\,000\,{\rm km\,s^{-1}}$. In *HST* Cycle 10, we had a snapshot programme to enhance the *HST* archive with 100–200 Wide Field Planetary Camera 2 (WFPC2) multicolour images of galaxies within approximately 20 Mpc. In the future, SNe discovered in these galaxies could have pre-explosion images available to constrain the nature of the progenitor stars. This strategy is now beginning to bear fruit, NGC 6207 was one of those targets and the pre-explosion site of SN 2004A was imaged in three filters.

In this paper, we present photometric and spectroscopic data of SN 2004A in Section 2 followed by an analysis of the photometry in Section 3.1, where an explosion date is estimated. We estimate the reddening towards the SN in Section 3.2 and obtain the expansion velocity in Section 3.3. The distance to NGC 6207 is not well known and only two distance estimates, which are both kinematic, exist in the literature. We estimate the distance using two further methods and compile the distances within the literature, in an attempt to improve the situation, in Section 4.3. Using the distance found, we then calculate the amount of nickel synthesized in the explosion in Section 5. We present the discovery of the progenitor in Section 6 and a discussion of the implications and conclusion in Sections 7 and 8, respectively. Throughout this work, we have assumed the galactic reddening laws of Cardelli, Clayton & Mathis (1989) with $R_V = 3.1$.

2 OBSERVATIONS

2.1 Ground-based photometry of SN 2004A

BVRI photometry was obtained shortly after discovery from the following telescopes: the 2.0-m Liverpool Telescope (LT), La Palma; the 4.2-m William Herschel Telescope (WHT), La Palma; and the Robotic Palomar 60-inch telescope (P60[1]; Cenko et al., in preparation) as part of the Caltech Core-Collapse Program[2] (CCCP; Gal-Yam et al. 2004, 2005; Gal-Yam et al., in preparation) The LT observations were taken with the optical CCD Camera, RATCam, using its Bessel *BV* and Sloan $r'i'$ filters. The data were reduced using the LT data reduction pipeline. The WHT observations were taken with the Auxiliary Port Imaging Camera (AUX), using its *BVRI* filters, and were reduced using standard techniques within IRAF. The frames were debiased and flat-fielded using dome flats from a few nights later. Details of the P60 camera and data reduction can be found in Rajala et al. (2005). A summary of these observations can be found in Table 1 as well as the results from the SN photometry.

The Johnson–Cousins *BVRI* magnitudes, in all epochs, were obtained using the aperture photometry task within the IRAF package DAOPHOT, and were calibrated using differential photometry. Unfortunately there were no standard fields taken on the same nights as the SN data, except with those taken on 2004 June 3, with the AUX. The AUX, with its 1024×1024 TEK CCD, has an unvignetted, circular field diameter of 1.8 arcmin, which meant that only stars A and B, from the SN 2004A field in Fig. 1, fell within the aperture. Because of the highly variable quality of the images, *both* stars A and B were not well observed in every epoch (mostly because of B being significantly fainter than the SN). We could have used only these two stars but decided instead to employ a two-step process. We first calibrated stars A and B from the AUX images, and then used them to calibrate the other stars in the field, using the night with the best-quality images, to create a catalogue from which the SN could then be calibrated. To this end stars A and B, and SN 2004A, were calibrated using the standard stars, SA 107 626 and 627. The night with the best quality images, 2004 April 24, was then chosen to represent our 'standard field'. The remainder of the stars, that were present and usable in all epochs, were calibrated using stars A and B. The stars calibrated in this way are numbered in Fig. 1 and their *BVRI* magnitudes are given in Table 2, where the numbers in brackets are the statistical errors. The magnitudes of the 'standard' stars, A–B and 1–15, are the simple average of the individual values determined from each calibration star from two different images, and the error is the standard deviation.

The catalogue in Table 2 was used to calibrate all the epochs in Table 1, except those from the *HST* and, as we have discussed, the AUX. The *BVRI* light curves are plotted in Fig. 2. The 'standard' stars were visible in the majority of the epochs although the field size and pointing of the LT meant that only stars A, B, 3, 6, 7, 8, 9 and 10 were used for the night of 2004 February 1 and stars A, B, 1, 7 and 8 for the night of 2004 August 30. The SN magnitudes are the simple average of the individual values determined from each calibration star, where any outliers that were greater than 2σ away from the mean were omitted. The statistical error, shown in brackets, is either the standard deviation or the combined error from each of the estimates, whichever was the greater.

In the course of calibrating our 'standard' field, the SN magnitudes for 2004 April 24, were also calibrated using only stars A

[1] http://www.astro.caltech.edu/~derekfox/P60/

[2] http://www.astro.caltech.edu/~avishay/cccp.html

Table 1. Journal and results of optical photometry of SN 2004A.

Date	JD (245 0000+)	Phase (d)	*B*	*V*	*R*	*I*	Telescope plus instrument
2004 February 01	3036.77	26	16.05 (0.05)	15.36 (0.03)	15.01 (0.02)	14.82 (0.03)	LT plus RATCam
2004 February 05	3040.92	30	16.27 (0.04)	15.52 (0.02)	15.05 (0.01)	14.79 (0.03)	P60
2004 February 06	3041.92	31	16.33 (0.09)	15.44 (0.03)	15.01 (0.02)	14.71 (0.03)	P60
2004 February 07	3042.92	32	16.23 (0.06)	15.49 (0.04)	15.02 (0.02)	14.77 (0.03)	P60
2004 February 08	3043.91	33	16.34 (0.06)	15.45 (0.04)	15.03 (0.02)	14.77 (0.05)	P60
2004 February 13	3048.90	38	15.92 (0.03)	15.17 (0.04)	14.89 (0.02)	14.69 (0.03)	P60
2004 February 15	3050.90	40	–	15.35 (0.02)	14.94 (0.01)	14.71 (0.04)	P60
2004 February 17	3052.89	42	16.27 (0.02)	15.32 (0.02)	14.98 (0.02)	14.68 (0.04)	P60
2004 February 18	3053.89	43	16.36 (0.04)	15.48 (0.05)	15.09 (0.04)	14.85 (0.08)	P60
2004 March 14	3078.84	68	16.43 (0.01)	15.31 (0.03)	14.91 (0.01)	14.61 (0.02)	P60
2004 March 23	3088.02	77	16.71 (0.04)	15.60 (0.07)	14.95 (0.05)	14.55 (0.12)	P60
2004 April 21	3116.97	106	16.97 (0.01)	15.76 (0.02)	15.27 (0.01)	14.89 (0.02)	P60
2004 April 24	3119.83	109	17.25 (0.01)	15.86 (0.02)	15.43 (0.01)	15.04 (0.01)	P60
2004 April 26	3121.83	111	17.15 (0.02)	16.13 (0.04)	–	14.98 (0.03)	P60
2004 April 27	3122.80	112	17.49 (0.01)	15.78 (0.03)	15.56 (0.01)	15.19 (0.01)	P60
2004 April 28	3123.79	113	17.41 (0.01)	16.27 (0.02)	15.66 (0.01)	15.23 (0.01)	P60
2004 April 29	3124.79	114	17.30 (0.02)	16.21 (0.02)	15.54 (0.02)	15.16 (0.03)	P60
2004 May 05	3130.84	120	18.11 (0.04)	–	–	–	P60
2004 June 03[a]	3160.49	150	19.04 (0.04)	17.68 (0.05)	16.93 (0.03)	16.44 (0.01)	WHT plus AUX
2004 August 30	3248.47	238	19.47 (0.12)	18.25 (0.04)	17.62 (0.04)	17.29 (0.03)	LT plus RATCam
2004 September 23	3271.65	261	19.95 (0.03)	19.02 (0.04)	–	17.60 (0.04)	*HST* plus ACS

Note. Figures in brackets give the statistical errors associated with the magnitudes.
[a]Observers were R. Østensen and C. R. Benn. LT = 2.0-m Liverpool Telescope, La Palma. P60 = Robotic Palomar 60-inch telescope, Palomar. WHT = 4.2-m William Herschel Telescope, La Palma.

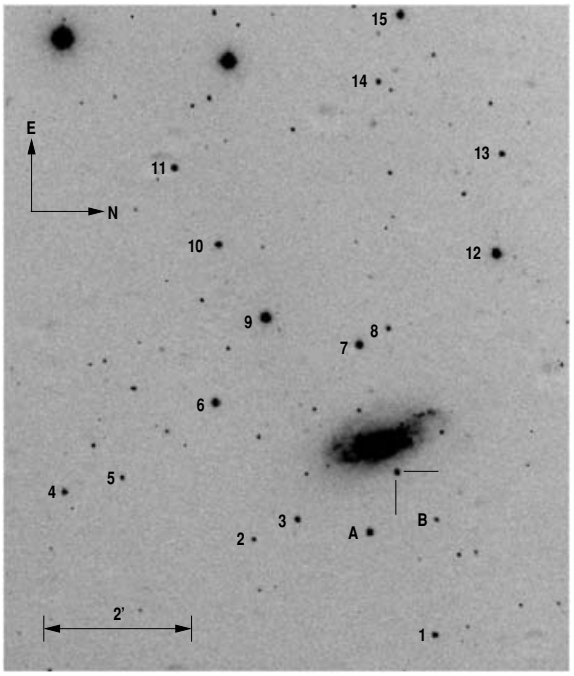

Figure 1. Finder chart for SN 2004A. The letters denote the stars that were calibrated from the WHT–AUX images. The numbers denote stars that were calibrated using stars A and B.

Table 2. Photometry of the stars in the field surrounding SN 2004A. The stars are labelled in the same way as in Fig. 1. Stars A and B were calibrated from the WHT–AUX images and the other numbered stars were then calibrated using stars A and B. The figures in brackets give the statistical errors associated with the magnitudes.

ID	*B*	*V*	*R*	*I*
A	15.959 (0.008)	15.195 (0.018)	14.736 (0.035)	14.322 (0.017)
B	18.081 (0.019)	17.560 (0.015)	17.267 (0.034)	16.943 (0.021)
1	16.546 (0.022)	15.901 (0.066)	15.541 (0.028)	15.213 (0.017)
2	17.664 (0.022)	17.104 (0.066)	16.791 (0.028)	16.548 (0.017)
3	16.283 (0.022)	15.563 (0.066)	15.169 (0.028)	14.842 (0.017)
4	16.527 (0.022)	15.898 (0.066)	15.565 (0.028)	15.275 (0.017)
5	17.808 (0.022)	16.989 (0.066)	16.535 (0.028)	16.173 (0.017)
6	14.914 (0.022)	14.242 (0.066)	13.889 (0.028)	13.562 (0.017)
7	14.558 (0.022)	13.966 (0.066)	13.639 (0.028)	13.355 (0.017)
8	16.971 (0.022)	16.305 (0.066)	15.950 (0.028)	15.696 (0.017)
9	13.868 (0.022)	13.016 (0.066)	12.548 (0.028)	12.157 (0.017)
10	15.756 (0.022)	15.135 (0.066)	14.800 (0.028)	14.483 (0.017)
11	16.093 (0.022)	15.140 (0.066)	14.620 (0.028)	14.165 (0.017)
12	14.165 (0.022)	13.127 (0.066)	12.575 (0.028)	12.111 (0.017)
13	16.675 (0.022)	15.999 (0.066)	15.624 (0.028)	15.309 (0.017)
14	16.739 (0.022)	16.012 (0.066)	15.614 (0.028)	15.270 (0.017)
15	14.583 (0.022)	14.050 (0.066)	13.757 (0.028)	13.508 (0.017)

and B. The difference between these magnitudes and those obtained using the catalogue, gave us an estimate of the systematic error introduced by the calibration, including the transformation from our 'standard' system to the AUX system. We therefore estimate the calibration error, for bands *BVRI*, to be 0.01, 0.12, 0.03 and 0.07, respectively.

The observations are from four different instrumental set-ups and filter systems; the LT, the P60 before 2004 March 14, the P60 after 2004 March 14, and the WHT. There are two instrumental set-ups for the P60 as its CCD was changed on 2004 March 14. The colour transformation plots of the instrumental magnitudes, from both the LT and the P60 pre-2004 March 14 systems, compared to the

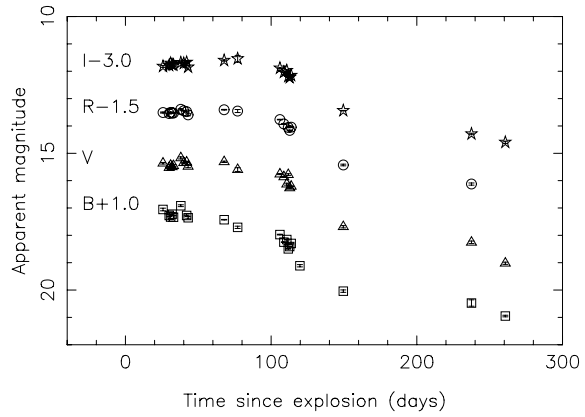

Figure 2. *BVRI* light curves of SN 2004A, which have been arbitrarily shifted in magnitude for clarity. There is a clear and well-developed plateau phase in each filter lasting around 80–100 d from the estimated explosion epoch.

Table 3. rms residuals assuming no colour transformations between the instrumental magnitudes and the intrinsic colours.

Transformation	*B*	*V*	*R*	*I*
AUX→Landolt	0.01	0.01	0.01	0.01
'Standard'→AUX	0.02	0.05	0.01	0.02
LT→'standard'	0.05	0.04	0.03	0.03
P60 (pre-040314)→'standard'	0.04	0.04	0.02	0.03

intrinsic colours of the 'standard' stars suggested that it was unnecessary to apply a colour correction to any of the *BVRI* magnitudes, to transform the instrumental magnitudes to our 'standard' system. We would, however, add caution to the *RI* magnitudes from the LT, as these are Sloan $r'i'$ magnitudes. The transformation from the $r'i'$ to the *RI* system was found to be problematic by Hendry et al. (2005). When the transformations were applied to the field stars the *RI* results were reliable, however, when the same transformations were applied to the SN they gave very unsatisfactory results. The authors suggested that the strong emission-line SN spectrum produced systematic differences in the colour terms compared to the stellar spectral energy distributions (SEDs). We believe that it is not advantageous to apply a colour correction to the Sloan $r'i'$ magnitudes here and we have retained them as pseudo-*RI* magnitudes. The two LT *RI* points are not deviant from the light curves in Figs 2 and 5, and the point in the tail also fits very well to both the other SN 2004A data and the extrapolated SN 1999em light curves, lending credence to this assumption. The rms of the residuals for each system, assuming no colour correction, are shown in Table 3. It is difficult to determine if a colour correction is needed to transform our 'standard' system to the Landolt system, because both the AUX images and our 'standard' field were only calibrated using two standards. The transformation plots, however, did not suggest that one was required.

The error introduced to the LT and the P60, pre-2004 March 14, magnitudes by assuming there was no colour correction, was estimated from the best linear fits to the transformation plots. These errors were comparable to the values for the gradient and offset, and often larger, and the reduced-χ^2 values were comparable to those for the null hypothesis, hence there is no value in applying them. As there are only two standard stars each for the transformations from our 'standard' system to the Landolt system, we were unable to estimate an error in this way. However, we have already estimated an error for the transformation from our 'standard' system to the AUX system, leaving only the AUX to Landolt transformation, where we have used the rms residual value to represent the error. We have added these errors in quadrature to the statistical error, hence this uncertainty is accounted for throughout the analysis in the forthcoming sections. We show that the major conclusions of this paper are not critically dependent on these uncertainties.

Table 4. Johnson–Cousins BVRI magnitudes, from SDSS DR4, for selected stars in the field of SN 2004A, using the same sequence as Fig. 1.

ID	*B*	*V*	*R*	*I*
A	16.083	15.264	14.796	14.364
3	16.422	15.684	15.263	14.885
6	15.039	14.349	13.955	13.575
7	14.748	14.136	13.787	13.381
9	16.338	13.941	12.560	12.090
10	15.891	15.257	14.897	14.510
12	16.437	14.002	12.599	12.046
15	14.705	14.175	13.874	13.545

The error introduced by the difference between the Cousins *RI* and the Sloan $r'i'$ filters was quantified using spectrophotometry, using the IRAF package SYNPHOT within STSDAS, applied to the only spectrum of SN 2004A. Using the rescaled spectrum (see Section 2.2), the differences $R - r'$ and $I - i'$ were -0.06 and 0.01, which are comparable to the estimated errors for *R* and well within the errors in *I*. SN 1999em at a similar phase also differed by consistent amounts. However, the differences between the SYNPHOT and LT Sloan $r'i'$ filters were not addressed. We do not have spectra from phases close to the LT photometry epochs so we used the spectra of SN 1999em to investigate these as they gave consistent results at around 40 d. At a phase of 23 d the differences were -0.02 and 0.03, and at 165 d they were -0.01 and -0.05, respectively. The errors estimated for the LT are large enough to account for any error introduced by the difference in the Cousin and Sloan filters. In any case there are only two LT epochs and the conclusions of this paper are not reliant on these points.

Since the data in this paper was reduced, calibrated and analysed, the Sloan Digital Sky Survey (SDSS) data release 4 (DR4) was made public. As a check, the photometry was redone using the standard sequence given in Table 4. Star A, which was one of the stars used to calibrate the 'standard' field, differs by: 0.12, 0.07, 0.06 and 0.04 mag in *BVRI*, respectively. The SN photometry calibrated using the SDSS catalogue (Table 4) is fainter over all the epochs and bands, with differences, averaged over all the epochs, of: 0.14, 0.12, 0.08 and 0.02 for each band. The differences in the light curves are, however, minimal. The calibration errors for using the catalogue in Table 2, as opposed to just stars A and B were: 0.01, 0.12, 0.03 and 0.07, for bands *BVRI*, respectively. These errors were added in quadrature to the errors derived from the LT and the P60, pre-2004 March 14, colour transformation equations, so will adequately cover the differences in the photometry. The main results on which the SDSS catalogue will have an effect are the standard candle method (SCM) distance estimate, and consequently the nickel mass. However, the SCM distance was found not to change significantly, increasing the overall distance to NGC 6207 by only 0.2 Mpc. Therefore, the analysis and conclusions of this paper are the same irrespective of the catalogue that is used. There are errors

Table 5. Details of optical spectrum of SN 2004A

Date	2004 February 18
JD (+245 0000)	3054.15
Phase	43 d
Range	3373–10380 Å
Resolution	10.6 Å
Telescope/Instrument	Keck/LRIS
Observer	Smartt/Maund

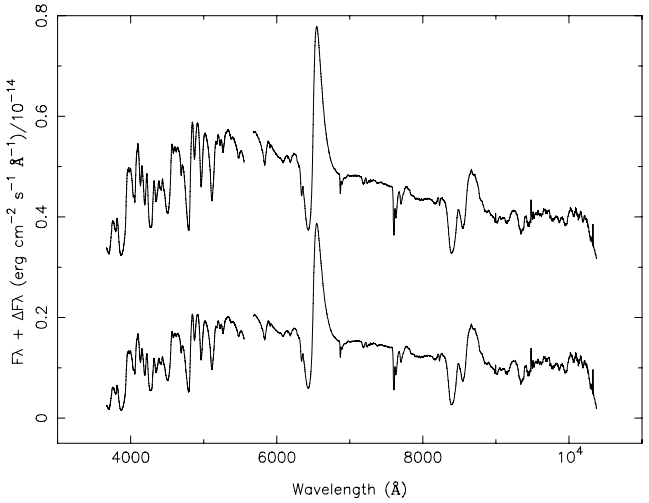

Figure 3. The original flux calibrated spectrum (bottom), showing a slightly flatter continuum below 6 000 AA, and the same spectrum with the linear scale function applied (top).

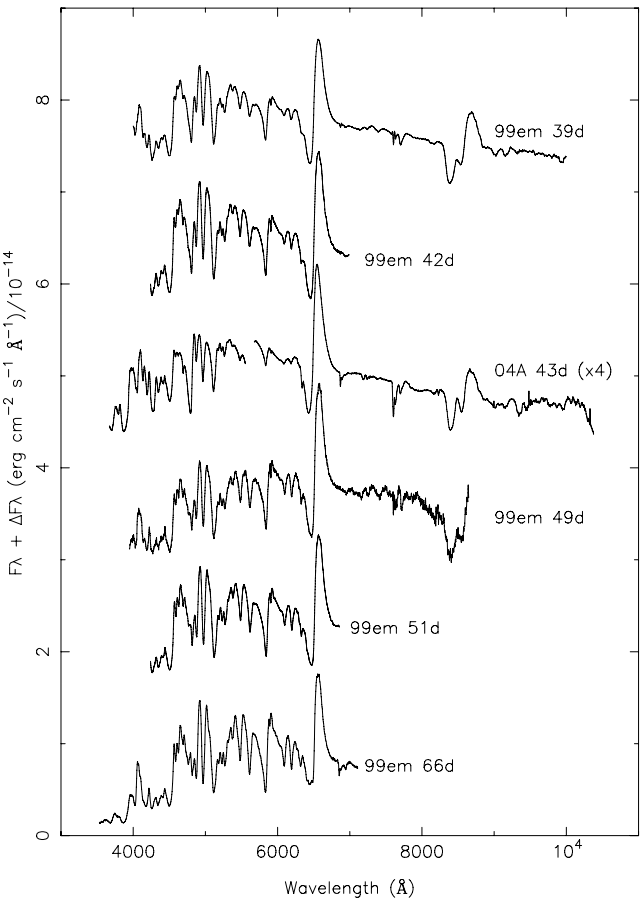

Figure 4. The scaled spectrum of SN 2004A compared with the spectra of SN 1999em (Leonard et al. 2002; Hamuy et al. 2001) over the range of plausible phases for SN 2004A, from the explosion epoch. The spectrum of SN 2004A has been further scaled for clarity.

associated with the transformation of the SDSS stellar magnitudes to the Johnson–Cousins filter system, so the SDSS catalogue in Table 4 is probably not any more reliable than the catalogue used here. Hence the photometry of SN 2004A from the SDSS catalogue, because of the errors in the transformation of the catalogue, is not any more reliable than the photometry presented here. Its agreement is reassuring though and makes the further analysis all the more robust.

2.2 Spectroscopy of SN 2004A

An optical spectrum of SN 2004A was obtained on 2004 February 18.65 UT, at a phase of ∼43 d (see Section 3.1), using the LRIS instrument on Keck. The details of the spectrum are given in Table 5. The spectrum was reduced using standard routines within IRAF. The frames were debiased, flat-fielded and extracted and then wavelength calibrated using Cu–Ar and Cu–Ne lamp spectra. The wavelength calibration was checked by determining the positions of the night sky lines and small adjustments were made. The spectra were then flux calibrated using spectrophotometric flux standards observed with the same instrumental set-up. The slit-width employed was 0.7 arcsec, hence the flux calibration is unlikely to give an accurate absolute scale. The continuum of the resulting spectra was visibly flat in the region lower than 6 000 AA (see Fig. 3, bottom), possibly indicating a problem with the flux calibration. We therefore used the *BVRI* photometry to adjust the flux calibration. Spectral *BVRI* magnitudes were calculated from the spectra using the IRAF package SYNPHOT within STSDAS. These magnitudes were compared to the observed photometric magnitudes. In order to match the photometric magnitudes, a linear scaling function (linear in flux and wavelength) was calculated and applied to the spectrum. The original flux calibrated spectrum and the scaled spectrum are shown in Fig. 3. The spectrum was read into the spectral analysis program DIPSO (Howarth et al. 2003) for further analysis.

The spectrum of SN 2004A is compared to that of the well-observed SN 1999em, in Fig. 4, over the plausible phases inferred from the observations of Itagaki (Nakano et al. 2004). The spectrum looks similar to those of SN 1999em at a similar phase and shows that the χ^2-fitting method (Section 3.1) may have overestimated the explosion epoch by a few days. The spectrum shows P-Cygni profiles and broad spectral features, indicative of the high velocities of the SN. The spectrum will be available through the SUSPECT[3] website.

2.3 *HST* Observations of NGC 6207

Observations of NGC 6207, before the explosion of SN 2004A, were taken with WFPC2 on board *HST* on two separate occasions through the filters F606W, F814W and F300W, as part of programs SNAP9042 and GO8632 (all details are given in Table 6). Further

[3] http://bruford.nhn.ou.edu/∼suspect/

Table 6. Summary of *HST* observations

	Date	Filter	Data set	Exposure (s)	Instrument	Program ID
Pre-explosion	2000 August 03	F300W	U67GA101B	1000	WFPC2	GO8632
	2001 July 02	F606W	U6EAD003B	460	WFPC2	SNAP9042
	2001 July 02	F814W	U6EAD001B	460	WFPC2	SNAP9042
Post-explosion	2004 September 23	F435W	J8NV02010	1400	ACS/WFC	GO9733
	2004 September 23	F555W	J8NV02020	1510	ACS/WFC	GO9733
	2004 September 23	F814W	J8NV02030	1360	ACS/WFC	GO9733

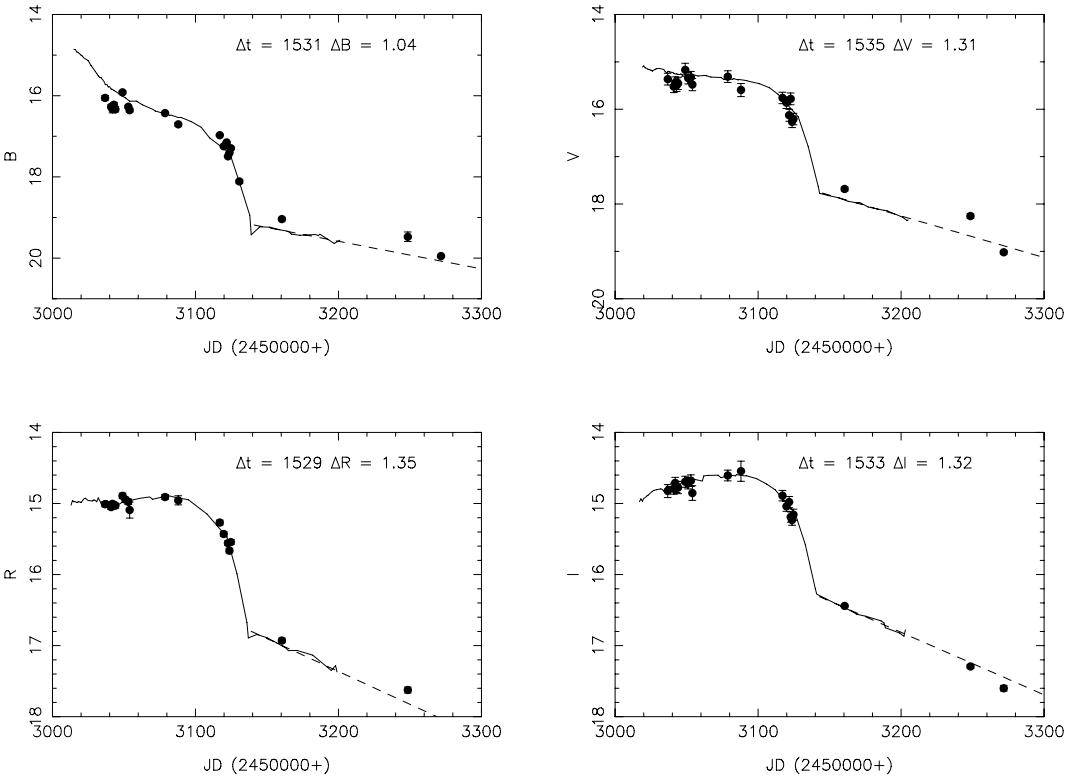

Figure 5. *BVRI* light curves of SN 2004A, shown with the filled circles, overplotted with the best-fitting light curve of SN 1999em, from Hamuy et al. (2001), shown with the solid line (which has been shifted by Δt days and Δm magnitudes). The reduced-χ^2 of the fit for the comparison of the *BVRI* light curves are: 23.10, 2.91, 2.30 and 0.74. The dashed line represents the best linear fit to the data in the tail of SN 1999em.

HST imaging was acquired with the Wide Field Camera (WFC) of the Advanced Camera for Surveys (ACS). SN 2004A was observed at an epoch ∼261 d after explosion using three filters F435W, F555W and F814W as part of program GO9733. These observations were acquired in order to determine a value of the reddening towards stars near the SN and to determine the exact location of the SN with respect to nearby stars. These images allowed the precise location of the SN to be determined on the pre-explosion observations. The target was placed close to the centre of chip WF1.

The on-the-fly re-calibrated (OTFR) ACS images were obtained from the Space Telescope European Coordinating Facility archive. Photometry was conducted on these frames using the new custom built ACS point spread function (PSF)-fitting photometry modules in the package DOLPHOT[4] (Dolphin 2000). This incorporates PSF fitting with model ACS PSFs, charge transfer efficiency (CTE), aperture corrections and transformation between the flight system magnitudes and standard Johnson–Cousins *BVI* filter bands. Stars, suitable for the brightest supergiants method (BSM) distance determination technique (see Section 4.2), were selected from the photometry output using the DOLPHOT object-type classification scheme. Objects that were classified by DOLPHOT as extended, blended or containing bad pixels were discarded, as they were probably blended stars or stars in crowded areas with PSF fit $\chi^2 > 2.5$.

The WFPC2 pre-explosion images were retrieved from the Space Telescope Science Institute archive, and calibrated via the OTFR pipeline. These observations were made in three bands F300W, F606W and F814W. The site of SN 2004A was located on the WF3 chip in all WFPC2 observations, which has a resolution of 0.1 arcsec per pixel. Aperture photometry was conducted using the IRAF package DAOPHOT and PSF photometry performed using the HSTPHOT package (Dolphin 2000). HSTPHOT includes corrections for chip-to-chip variations, CTE and transformations from WFPC2 instrumental magnitudes to the standard Johnson–Cousins magnitude system.

[4] http://purcell.as.arizona.edu/dolphot/

Table 7. Results from the χ^2-fitting algorithm which adjusts the time, Δt, and apparent magnitude, Δm, of the 'model' light curve (SN 1999em) to find the best fit to the data points of SN 2004A, where ν = number of data points – number of degrees of freedom.

Filter	Reduced-χ^2	ν	Δt (d)	Δm
B	23.10	18	1531 (3)	1.04 (0.08)
V	2.91	18	1535 (3)	1.31 (0.08)
R	2.30	17	1529 (3)	1.35 (0.04)
I	0.74	18	1533 (3)	1.32 (0.04)
BVRI			1532 (3)	

3 ANALYSIS OF THE EVOLUTION OF SN 2004A

3.1 Explosion epoch

Using a similar method to Hendry et al. (2005), the light curve of SN 2004A was compared to that of SN 1999em (Hamuy et al. 2001), which is the most fully studied normal SN II-P to date, to obtain an estimate of the explosion epoch. This was accomplished using a χ^2-fitting algorithm to adjust the time and apparent magnitude of the 'model' light curve of SN 1999em, to find the best fit to the data points of SN 2004A. The SN 2004A errors used in this analysis were the statistical plus the systematic error discussed in Section 2.1. The last two points in the tail of SN 2004A were not included in the fit as there was insufficient data from the SN 1999em light curve, as can be seen from Fig. 5. The *BVRI* best fits are shown in Fig. 5 with the shift in time, Δt, and apparent magnitude, Δm, inset in each figure. The results from the χ^2-fitting algorithmare shown in Table 7.

The reduced-χ^2 values are exceedingly large for the *B* band and is indicative of a poor fit. The fit by eye looks quite poor as there is a large scatter about the light curve. The statistical and systematic errors are small in the *B* band, but the scatter suggests that this may have been underestimated. The light curves, although they have the same general shape, are different in the early part of the *B*-band light curve and in the tail. The early SN 2004A light curve appears to be flatter and the tail slightly more luminous, increasing the χ^2 value. The *V*-band fit also has a reasonably high reduced-χ^2, although it is lower than that of the *B*-band fit. There is a reasonably large scatter around the light curve, however, the shape of the light curves are more consistent than in the *B* band. The *RI* bands visually appear to be good fits and their reduced-χ^2 values are correspondingly lower, although the value for the *R* band is still on the high side. The points in the SN 2004A tail are also fitted well by the SN 1999em light curve and the later points, omitted from the fit, are also in agreement with the extrapolated light curve, shown with the dashed line. There is some scatter in the points compared to SN 1999em, which is due to the variable quality of the imaging for this event and very unlikely to be due any intrinsic brightness variations.

The reduced-χ^2 values were too large in the *BVR* bands to be able to do a sensible error analysis using the confidence limits. We estimated the errors instead, in all bands, by first rounding Δt to the nearest day and then fitting the light curves by eye to obtain a realistic range of values for Δt and Δm. These ranges are the errors quoted, in brackets, in Table 7. The *I*-band fit was sufficiently good to estimate an error from the confidence limits. Using the 2σ confidence limit, we estimate, $\Delta t(I) = 1532.5^{+2.5}_{-3.0}$, rounded to the nearest half day, and $\Delta I = 1.32^{+0.04}_{-0.08}$, which is in agreement with what was found by eye.

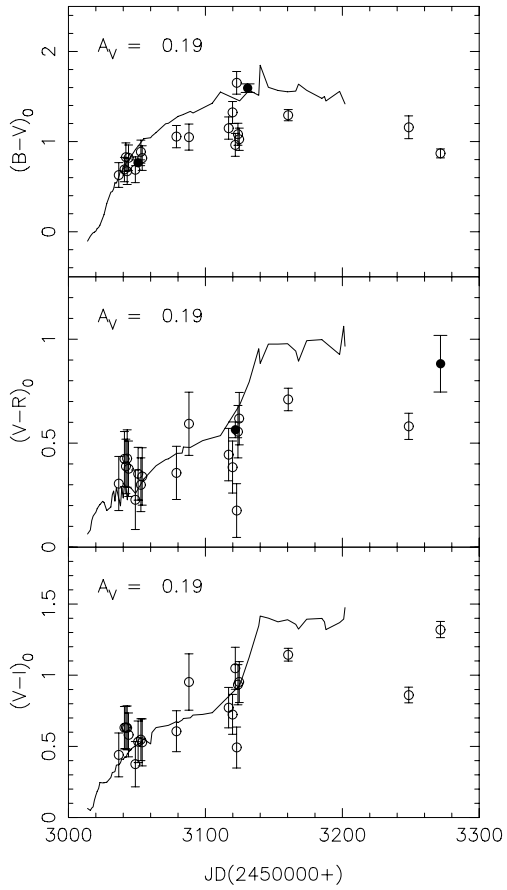

Figure 6. Colour evolution of SN 2004A (points) compared with that of SN 1999em (solid line) for $A_V = 0.19$.

The explosion epoch of SN 2004A, using this method, was estimated to be JD 245 3011 ± 3, which corresponds to 2004 January 6. This was achieved using the simple average of Δt, for *BVRI*, and the explosion epoch of SN 1999em, which was estimated to be JD 245 1478.8 ± 0.5 by Hamuy et al. (2001), within 2 d of Elmhamdi et al. (2003b). The error in the explosion epoch was estimated from the errors in the weighted average of Δt and in the SN 1999em explosion date. The error of ± 3 d is the error on the fit and does not reflect the systematic error that is introduced by assuming that both SN 2004A and SN 1999em are intrinsically the same. We can, however, estimate a more appropriate error from observations. We can put a hard limits on the earliest and latest possible explosion date of SN 2004A by using the observations of K. Itagaki (Nakano et al. 2004). The SN was discovered by Itagaki (Nakano et al. 2004) on January 9.84 UT and it was not seen on Itagaki's previous observations of 2003 December 27, which have a limiting magnitude of 18. The explosion epoch found by the χ^2-fitting method is consistent with this limit, which gives us a robust uncertainty range for the explosion epoch of JD $245\,3011^{+3}_{-10}$

3.2 Reddening estimate towards SN 2004A

3.2.1 Reddening towards the neighbouring stars

BVI ACS photometry (see Section 2.3) was used to estimate the reddening towards SN 2004A. $B - V$ and $V - I$ colours of stars within 6 arcsec of SN 2004A were compared with the intrinsic supergiant colour sequence of Drilling & Landolt (2000). The reddening was calculated using a χ^2-minimization of the displacement of the stars

Table 8. Reduced-χ^2 values from the comparison of the colour evolutions of SNe 2004A and 1999em, for an extinction of $E(B-V) = 0.06 \pm 0.03$ for SN 2004A, estimated from the neighbouring stars.

	Reduced-χ^2	ν
$B-V$	2.035	12
$V-R$	0.940	13
$V-I$	0.969	13

from the intrinsic supergiant colour sequence, for a range of values of $E(B-V)$. The reddening vector, in the $B-V/V-I$ colour plane, assumed the reddening laws of Cardelli et al. (1989) with $R_V = 3.1$. Using this method, the reddening was estimated as $E(B-V) = 0.06 \pm 0.03$, which corresponds to $A_U = 0.29 \pm 0.15$, $A_V = 0.19 \pm 0.09$ and $A_I = 0.09 \pm 0.05$.

3.2.2 Reddening and the colour evolution of SN 2004A

The reddening towards SNe can also be estimated from a comparison between the colour evolutions of the SN in question and another well-studied SN, for which the reddening is known to some degree of accuracy. This method assumes that SNe II-P all reach the same intrinsic colour towards the end of the plateau phase. This is based on the assumption that the opacity of SNe II-P is dominated by electron scattering, therefore the SN should reach the temperature of hydrogen recombination at the end of the plateau phase (Eastman, Schmidt & Kirshner 1996; Hamuy 2004a). Unfortunately, the photometry was not accurate enough to estimate an independent reddening towards the SN, although we could ascertain whether the estimate from the surrounding stars and the colour evolution were consistent.

We compared the colour evolution of SN 2004A with that of SN 1999em, following a similar approach to Hendry et al. (2005), who adopted a reddening of $E(B-V) = 0.075 \pm 0.025$ for SN 1999em (Baron et al. 2000). The colour curves of SN 1999em were first dereddened using this value and were then shifted in time using the weighted average of Δt discussed in Section 3.1. The colour curves of SN 2004A were then dereddened using the estimate from the neighbouring stars estimated here. The comparison of the colour evolutions are shown in Fig. 6 and the reduced-χ^2 values are listed in Table 8. The χ^2-fit was restricted to JD <245 3120, the end of the plateau.

The reduced-χ^2 values are indicative of a good fit for the $V-R$ and $V-I$ colours, although the error bars are quite large. The quoted uncertainties are a combination of the statistical errors from the photometry and the errors associated with the calibration discussed in Section 2.1. The fits show that, even though we could not obtain an independent reddening estimate, the colour evolution is consistent with an extinction of $E(B-V) = 0.06 \pm 0.03$. As in Hamuy (2004a) and Hendry et al. (2005), we find that the $B-V$ is not as well behaved and has a higher χ^2 value. Although the $B-V$ fit is poorer, it is still consistent with the reddening towards the neighbouring stars.

3.3 Expansion velocity

We have used the method of Hendry et al. (2005), which was found to be consistent with other methods (Hamuy et al. 2001; Leonard et al. 2002; Elmhamdi et al. 2003b), to measure the expansion velocity of the ejecta of SN 2004A from our spectrum at 43-d post-explosion. The expansion velocity was measured from the minimum of the blueshifted absorption trough of the Fe II λ5169 line. The absorption trough was fitted by three Gaussians using the Emission Line Fitting package (ELF) within the Starlink spectral analysis package DIPSO. The minimum was found from the three Gaussian fit and the error was estimated from the difference between this and a single Gaussian fit. We found the expansion velocity, of the ejecta of SN 2004A at 43 d, to be $v = 4123 \pm 93$ km s^{-1}, using the NASA/IPAC Extragalactic Data base[5] (NED) recessional velocity of 852 km s^{-1} for NGC 6207. A comparison of the expansion velocities of SN 2004A and other SNe II-P is shown in Fig. 7. The SN 2004A expansion velocity is consistent with other normal SNe II-P, as we would expect from the appearance of the spectral features in Fig. 4.

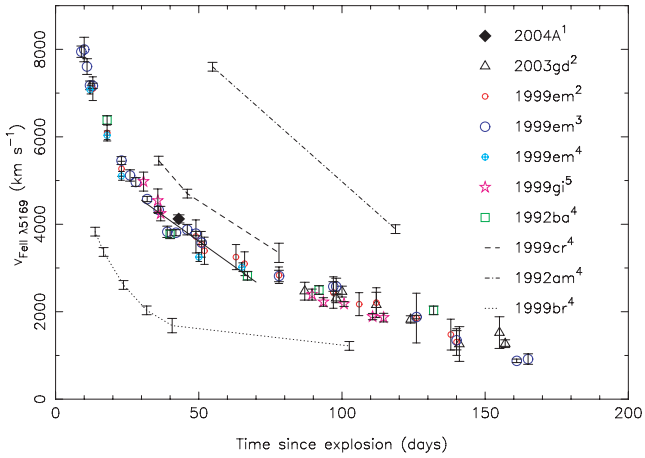

Figure 7. Velocity evolution of SN 2004A compared with other similar SNe II-P (1992ba, 1999em, 1999gi and 2003gd: plotted points) and contrasting SNe II-P (1999cr, 1992am and 1999br: dashed/dotted curves). The solid line is the best fit to the similar SNe II-P velocities between 30 and 70 d. The superscripts in the figure denote the source of the velocity measurements: (1) this paper, (2) Hendry et al. (2005) (3) Leonard et al. (2002), (4) Hamuy et al. (2001) and (5) Leonard et al. (2002).

4 DISTANCE ESTIMATES TO NGC 6207

4.1 Type II-P standard candle method distance estimate

Although SNe II-P shows a wide range of luminosities at all epochs, the velocities of their ejecta and their bolometric luminosities, during the plateau phase, are highly correlated. This correlation allowed Hamuy & Pinto (2002) to formulate an SCM for SNe II-P, which can be solved for the Hubble Constant provided a suitable distance calibrator is known. Hamuy in two further papers (Hamuy 2004a,b) confirmed the SCM, using a sample of 24 SNe II-P, and calibrated the Hubble diagram with known Cepheid distances to four of these SNe. Hamuy (2004b) calculated the Hubble constant, using V and I data, to be $H_0(V) = 75 \pm 7$ and $H_0(I) = 65 \pm 12$ km s^{-1} Mpc^{-1}. In this paper, we use the weighted average of these results, $H_0 = 72 \pm 6$ km s^{-1} Mpc^{-1}, which is comparable to $H_0 = 71 \pm 2$ km s^{-1} Mpc^{-1} derived as part of the *HST* Key Project using SNe Ia (Freedman et al. 2001).

[5] http://nedwww.ipac.caltech.edu/

We used equations (5) and (6) from Hamuy (2004b) conversely to estimate the distance to SN 2004A: equations (1) and (2):

$$D(V) = \frac{10^{(1/5)[V_{50} - A_V + 6.249(\pm 1.35)\log(v_{50}/5000) + 1.464(\pm 0.15)]}}{H_0} \quad (1)$$

and

$$D(I) = \frac{10^{(1/5)[I_{50} - A_I + 5.445(\pm 0.91)\log(v_{50}/5000) + 1.923(\pm 0.11)]}}{H_0}, \quad (2)$$

where V_{50}, I_{50} and v_{50} are the V and I magnitudes, and the expansion velocity, in km s^{-1}, at a phase of 50 d. The VI magnitudes and velocity of SN 2004A is known for a phase of 43 d, so in order to use the SCM we were required to interpolate or extrapolate these quantities to 7-d later.

There is quite a large scatter in the V- and I-band light curves so we fitted a straight line to the data between 20 and 80 d to allow us to estimate $V_{50} = 15.41 \pm 0.17$ and $I_{50} = 14.68 \pm 0.13$. The errors are from the error in the fit and amply account for the errors in the photometry and the explosion date. Unfortunately we only have one spectrum, so we were unable to extrapolate the SN 2004A velocity using data from the SN alone. In order to estimate the velocity at 50 d, we used the locus of similar SNe II-P velocities, which are consistent with that of SN 2004A (Fig. 7), to obtain an average velocity evolution. None of the SNe studied here deviate from this locus, so it is reasonable to assume that SN 2004A will also follow a similar evolution. We fitted a straight line to the velocities between 30 and 70 d and used this to project the velocity to 50 d, estimating $v_{50} = 3795^{+210}_{-502}$ km s^{-1}. The errors are a combination of the errors in the fit, the explosion date and the velocity at 43 d. The straight line fit is shown in Fig. 7 by a solid line.

Using these parameters, the reddening calculated in Section 3.2 and equations (1) and (2), we find $D(V) = 21.40^{+3.69}_{-4.89}$ and $D(I) = 20.67^{+2.89}_{-3.96}$ Mpc, where the error is statistical and comes from combining the uncertainties of each parameter in the SCM equations. A straight average of these results gives a distance of $D = 21.0^{+4.1}_{-4.5}$ Mpc, where the error is estimated from the limits of $D(V)$ and $D(I)$.

4.2 Brightest supergiant distance estimate using *HST* photometry

The brightest supergiants distance method (BSM) uses the correlation between the average luminosity of a galaxy's brightest supergiants and the host galaxy luminosity. This average luminosity should be independent of the host galaxy luminosity for there to be no distance degeneracy (Rozanski & Rowan-Robinson 1994). We have used the method of Sohn & Davidge (1996) to determine the magnitude of the brightest supergiants and the calibrations of both Rozanski & Rowan-Robinson (1994) and Karachentsev & Tikhonov (1994) to determine the distance. Sohn & Davidge (1996) divided the supergiants of M74 into red and blue using their $V - R$ colours, assuming $V - R = 0.5$ as the boundary between the red and blue supergiants. Taking into account M74's foreground reddening, this colour corresponds approximately to an F8 supergiant Drilling & Landolt (2000, table 15.7). The brightest supergiants were then found from their luminosity functions by estimating the number of foreground stars in each bin. The brightest bin with an excess of supergiants will also statistically contain the brightest supergiants. This effectively removes the contamination from foreground stars, which cause the distance to be underestimated. In this work, we have used an excess of 2σ to indicate a significant detection.

Table 9. *VI*-band luminosity functions of RSGs in NGC 6207, stars in a 149 × 92 arcsec^2 field adjacent to NGC 6207 and predicted foreground stars from Bahcall & Soneira (1981) field 16.

V	$n_{\rm RSG}$	$n_{\rm field}$	$n_{\rm fg}$
18–19	0	0	–
19–20	0	0	–
20–21	3	2	–
21–22	2	1	–
22–23	4	3	–
23–24	35	5	–
24–25	116	7	–
25–26	786	19	–
26–27	3066	98	–
I	$n_{\rm RSG}$	$n_{\rm field}$	$n_{\rm fg}$
18–19	1	0	1.50
19–20	5	3	2.02
20–21	2	4	2.60
21–22	7	4	3.20
22–23	57	4	3.71
23–24	442	7	3.63
24–25	1453	16	4.30
25–26	1921	55	4.60
26–27	128	36	–

The *HST* (ACS, see Section 2.3) photometry was first dereddened using the foreground extinction towards NGC 6207 from Schlegel, Finkbeiner & Davis (1998), accessed through the NED interface. The supergiants were divided into red and blue using their $V - I$ colours and the intrinsic colour of F8 type supergiants, which is $V - I = 0.72$ from Drilling & Landolt (2000,table 15.7). We have assumed that supergiants with $V - I \geqslant 0.72$ are RSGs and supergiants with $V - I < 0.72$ are BSGs. The number of foreground stars were estimated using Bahcall & Soneira (1981) field 16, which is the nearest field to NGC 6207. As SN 2004A was placed close to the centre of chip WF1 of ACS, the main body of the galaxy was contained on WF1. Hence, we could use the star counts on the other CCD to first check the predicted star counts and secondly to help identify the bin with the statistical excess in V. The galaxy disc and halo may well extend on to the WF2 chip, but it served as a useful check. We wished to identify the brightest supergiants in V using the field stars, both because the calibrations for RSGs are in V and Bahcall & Soneira (1981) do not have predictions for stars in this band. Both the predicted star counts and the number of field stars were scaled to the field of view of the galaxy data used (149 × 92 arcsec^2). The luminosity functions for red and blue supergiants are given in Tables 9 and 10, and plotted in Figs 8 and 9, respectively.

The predicted star counts and the number of field stars are in good agreement for magnitudes less than 23. A significant statistical excess of RSGs was found in the range $I = 22$–23 and BSGs in the range in $B = 22$–23. The three RSGs that were brightest in V, in the centre of the range $I = 22$–23, have an average of $V = 23.10$. This agrees well with the bin in the V-band luminosity function, which appears to have a statistical excess when compared to the field star count. We also fitted a linear function to plots of I against V, to convert our I magnitude to V. The results were consistent with the V-band luminosity function, so the bin $V = 23$–24 was taken to contain the brightest RSGs in V. The brightest RSGs and BSGs

Table 10. *B*-band luminosity functions of BSGs in NGC 6207, stars in a 149 × 92 arcsec^2 field adjacent to NGC 6207 and predicted foreground stars from Bahcall & Soneira (1981) field 16.

B	$n_{\rm BSG}$	$n_{\rm field}$	$n_{\rm fg}$
18–19	0	0	0.50
19–20	0	0	0.68
20–21	0	1	0.89
21–22	1	1	1.12
22–23	12	0	1.36
23–24	114	5	1.61
24–25	679	2	1.87
25–26	2656	9	2.14
26–27	4961	41	–

were therefore taken to have $V = 23.5 \pm 0.5$ and $B = 22.5 \pm 0.5$, respectively.

We first calculated the distance using the calibrations of Rozanski & Rowan-Robinson (1994) with $B_0^T = 11.16$, which is the face-on total apparent magnitude of NGC 6207 corrected for Galactic extinction, and for the inclination of NGC 6207, from the Lyon-Meudon Extragalactic Data base[6] (LEDA). We used an iterative approach with the calibrations from Rozanski & Rowan-Robinson (1994) using $M_B^{\rm gal} = -19.74$, which has been corrected to $H_0 = 72$ km s^{-1} Mpc^{-1}, also from LEDA. The results are listed in Table 11, where 10(a) and (d) are for RSGs and 10(c) and (f) are for BSGs. The errors on the distance moduli, and the corresponding distances, are a combination of the errors associated with the regressions of Rozanski & Rowan-Robinson (1994, table 5), and errors in quadrature for the size of the bin and the reddening. The simple averages give a distance modulus of $\mu = 31.64^{+0.33}_{-0.40}$, and distance of $D = 21.40^{+3.38}_{-3.66}$ Mpc, where the errors reflect the range of the individual values calculated.

The calibrations given in equations (1) and (2) of Karachentsev & Tikhonov (1994) are of the same form as the regressions 10(a) and (c) of Rozanski & Rowan-Robinson (1994). We used the same iterative approach here, although we used $B_0^T = 11.74$, which is not corrected for the galaxy's inclination, to be consistent with the data used to find the relationships. The distance moduli found were $\mu(V) = 31.84 \pm 0.59$ and $\mu(B) = 32.14 \pm 0.59$, corresponding to $D(V) = 23.32 \pm 6.34$ and $D(B) = 26.79 \pm 7.28$ Mpc. The errors are a combination of the errors associated with the regressions, the size of the bin and the reddening. The averages give $\mu = 31.99 \pm 0.15$ and $D = 25.06 \pm 1.74$ Mpc, where the errors again reflect the range of the individual values calculated.

4.3 Summary of distance estimates

A summary of distances to NGC 6207 from three different methods is listed in Table 12. As well our SCM and BSM estimates, derived in Sections 4.1 and 4.2, we have collated two kinematic distance estimates from the literature. The distance from Tully (1988) uses a heliocentric velocity of 852 km s^{-1} and the Tully & Shaya (1984) model for infall on to the Virgo cluster. The distance from LEDA uses a heliocentric velocity of 851 km s^{-1} and instead uses the Theureau et al. (1998) model for infall on to the Virgo cluster. The values have been corrected for a Hubble constant of $H_0 =$ 72 km s^{-1} Mpc^{-1}, in keeping with the rest of this paper. The simple mean of these kinematic distances is $D = 16.6 \pm 3.3$ Mpc, where the error is a combination of the standard deviation of the distances and the uncertainty resulting from the cosmic thermal velocity dispersion of 187 km s^{-1} (Tonry et al. 2000). The accuracy of kinematic distances is limited not only by the observed velocity dispersion around the Hubble Flow, but also on an accurate model to account for the infall on to Virgo and the Great Attractor, hence there is a large uncertainty associated with this method. Table 12 also gives the simple mean of the BSM estimate, where the error reflects the range of individual values estimated.

The BSM distance estimate yielded fairly consistent results for NGC 6207, although they had large errors associated with them. The

[6] http://leda.univ-lyon1.fr

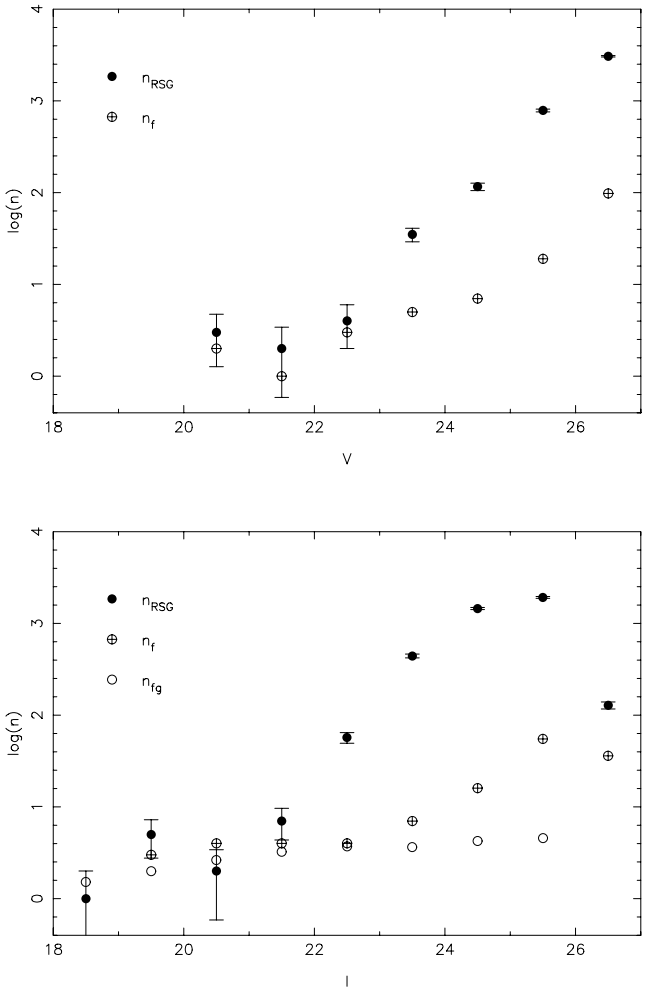

Figure 8. *VI*-band luminosity functions for RSGs in NGC 6207, field stars adjacent to NGC 6207 and predicted stars from Bahcall & Soneira (1981) field 16. There are no predicted star counts in the V band as they are not included in Bahcall & Soneira (1981).

Table 11. Results of the brightest supergiants distance estimate for NGC 6207 using Rozanski & Rowan-Robinson (1994). See Section 4.2 for details.

	10(a)	10(c)	10(d)	10(f)
μ	31.97 (0.77)	31.70 (1.03)	31.63 (0.74)	31.24 (1.01)
D (Mpc)	24.78 (8.79)	21.89 (10.38)	21.19 (7.22)	17.74 (8.25)

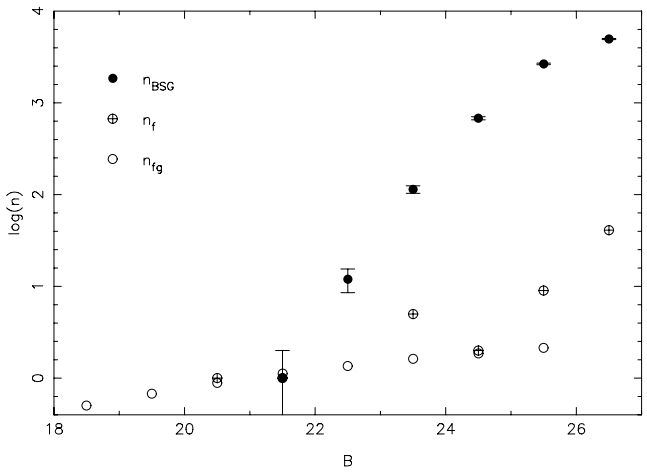

Figure 9. *B*-band luminosity function for BSGs in NGC 6207, field stars adjacent to NGC 6207 and predicted stars from Bahcall & Soneira (1981) field 16.

Table 12. Summary of distance estimates to NGC 6207. The estimated uncertainties are given in parentheses.

Method	Source	Distance (Mpc)	Mean
Standard candle	1	21.0 (4.3)	21.0 (4.3)
Brightest supergiants	1	21.4 (3.5)	23.2 (4.5)
	1	25.1 (1.7)	
Kinematic	2	18.1	16.6 (3.3)
	3	15.1	
Mean			20.3 (3.4)

(1) this paper, (2) Tully (1988), (3) LEDA.

individual estimates range from 17.7–26.8 Mpc, spanning 9.1 Mpc, over both the calibrations from Rozanski & Rowan-Robinson (1994) and Karachentsev & Tikhonov (1994). The standard deviations for each of these calibrations were 2.9 and 2.5 Mpc, respectively, which are high compared to the standard deviations that are usual for this method. Rozanski & Rowan-Robinson (1994) tested this method for several galaxies, with distances less than 5 Mpc, using the same four relationships as we have used here. They found standard deviations of around 0.4 Mpc with the exception of 1.7 Mpc for NGC 4395. In addition to the tests of Rozanski & Rowan-Robinson (1994), M74 was found to be at a distance of 7.7 Mpc with a standard deviation of 0.8 Mpc using these calibrations (see Hendry et al. 2005). The data used to produce these calibrations were all below ∼7 Mpc, therefore there could be a problem with extrapolating this relationship to higher distances. The accuracy of this method decreases as the distance increases because of contamination by unresolved clusters, and the calibrations themselves were found using data with distances less than ∼7 Mpc.

The distance estimates range from 15.1 to 25.1 Mpc, which spans 10 Mpc over all the methods, illustrating the inherent problems with distance estimation. All of these methods have problems and large errors associated with them. A full, in depth discussion of these problems can be found in Hendry et al. (2005). In order to obtain a distance, which is not biased towards any one method, we have taken a simple mean of the average results from each method to find the distance to NGC 6207. We find the distance to NGC 6207 to be $D = 20.3 \pm 3.4$ Mpc, where the error is the standard deviation of the averages of the individual methods.

5 ESTIMATE OF EJECTED ^{56}NI MASS

The light curves of SN 2004A and SN 1999em in Fig. 5 are very similar, although the tail of SN 2004A may be slightly brighter. We would therefore expect the nickel mass to be comparable to $M_{\rm Ni} = 0.048\,{\rm M}_{\odot}$, the nickel mass of SN 1999em from Hamuy (2003), which is corrected for the revised distance from Leonard et al. (2003), as discussed in Hendry et al. (2005). We have used the same three methods as Hendry et al. (2005) to find the mass of ^{56}Ni produced by SN 2004A. First of all it was estimated using the bolometric luminosity of the exponential tail (Hamuy 2003), secondly using a direct comparison with the light curve of SN 1987A and lastly using the 'steepness of decline' correlation, a new though unconfirmed method (Elmhamdi, Chugai & Danziger 2003a).

5.1 Nickel mass from bolometric luminosity of exponential tail

Hamuy (2003) derived $M_{\rm Ni}$ from the bolometric luminosity of the exponential tail, assuming that all of the γ-rays resulting from the ^{56} Co $\rightarrow ^{56}$Fe decay are fully thermalized. We first converted our V-band photometry in the tail to bolometric luminosities using equation (1) of Hamuy (2003), given here in equation (3). The bolometric correction is BC $= 0.26 \pm 0.06$ and the additive constant converts from Vega magnitudes to cgs units (Hamuy 2001, 2003). We have used the reddening and distance derived in Sections 3.2 and 4.3, respectively.

$$\log\left(\frac{L}{\rm erg\ s^{-1}}\right) = \frac{-(V - A_V + {\rm BC}) + 5\log D - 8.14}{2.5} \qquad (3)$$

and

$$M_{\rm Ni} = 7.866 \times 10^{-44} L \exp\left[\frac{(t - t_0)/(1 + z) - \tau_{\rm Ni}}{\tau_{\rm Co}}\right] {\rm M}_{\odot}. \qquad (4)$$

The nickel mass was then found using equation (2) of Hamuy (2003), given here in equation (4), where t_0 is the explosion epoch, $\tau_{\rm Ni} = 6.1$ d is the half-life of ^{56}Ni and $\tau_{\rm Co} = 111.26$ d is the half-life of ^{56}Co. We have used the explosion epoch derived in Section 3.1 and the redshift is from NED.

Using this method, we estimated $M_{\rm Ni}$ for each of the three points in the tail. We further estimated the range of possible values that this mass can possibly obtain, using the errors for each parameter. A simple average of the $M_{\rm Ni}$ results gives $M_{\rm Ni} = 0.050^{+0.040}_{-0.020}$, which is comparable to the nickel mass of SN 1999em as we expected. The error was calculated from the average of the extremes of the nickel mass values and not from the standard deviation, which was $0.013\,{\rm M}_{\odot}$, as the standard deviation only reflects the scatter in V-band magnitudes in the tail. This method is strongly dependent on the explosion epoch, extinction and the distance. Although the explosion epoch is fairly well known, there is a large uncertainty associated with distance and the V-band photometry, hence the large error.

5.2 Nickel mass from a direct comparison to SN 1987A light curve

The nickel mass was also estimated from the difference in the pseudo-bolometric (UVOIR) light curves of SN 2004A and SN 1987A, assuming the same γ-ray deposition. A χ^2-fitting algorithm was used to shift the light curve of SN 1987A on to that of SN 2004A

to find the best fit. When constructing the light curve of SN 1987A a distance of 50 kpc was adopted. The difference in log luminosity was found to be $\log(L^{87A}/L) = 0.247 \pm 0.030$. Equation (5) was then used to scale the nickel mass of SN 1987A, which was taken to be $0.075\,M_\odot$ (e.g. Turatto et al. 1998), to estimate that of SN 2004A.

$$M_{\rm Ni} = 0.075 \times \left(\frac{L}{L^{87A}}\right) M_\odot \quad (5)$$

In this way we find that $M_{\rm Ni} = 0.042^{+0.017}_{-0.013}\,M_\odot$, where the error is the combined error from the fit, the uncertainty in the explosion date and the distance. This method is dependent on two assumptions, one is the distance to the SN and the error in the nickel mass amply accounts for the distance uncertainty. The second is the assumption that both SNe have similar γ-ray escape fractions deposition rates. The validity of this cannot be tested with the current data, and this assumption is likely to lead to larger errors than the distance uncertainty.

5.3 Nickel mass from 'steepness of decline' correlation

Elmhamdi et al. (2003b) reported a correlation between the rate of decline in the V band, from the plateau to the tail, and the nickel mass estimated from the SN 1987A method. The advantage with this method is that it is independent of distance and explosion epoch, however, it does require a reasonably well-populated light curve and at the moment is an unconfirmed method. The authors defined a 'steepness' parameter, S, which is the maximum gradient during the transition in mag d^{-1}. A sample of 10 SNe II-P were used to determine the best linear fit. We have re-examined the results of Elmhamdi et al. (2003b) and derive the relationship given in equation (6).

$$\log\left(\frac{M_{\rm Ni}}{M_\odot}\right) = -6.9935(\pm 0.3791)S - 0.7383(\pm 0.0355). \quad (6)$$

Unfortunately, the light curve of SN 2004A is quite sparse so we could only put limits on the nickel mass using this method. We fitted a series of straight lines to the data to find the maximum and minimum values of S, which were plausible. The 'steepness' parameter for SN 2004A, using this method, was found to be in the range 0.07–0.21, which corresponds to $M_{\rm Ni} = 0.006 - 0.056\,M_\odot$, which is consistent with the first two methods.

5.4 Discussion of nickel mass estimate

The Hamuy (2003) and the direct comparison methods give consistent results of $M_{\rm Ni} = 0.050^{+0.040}_{-0.020}$ and $0.042^{+0.017}_{-0.013}\,M_\odot$, which are comparable to the nickel mass of SN 1999em, as we would expect from the appearance of the light curve and the spectra. These methods are, however, both dependent on the distance, although the errors sufficiently accommodate this. The method of Hamuy (2003) assumes that the γ-rays are fully thermalized, but this is not unreasonable as the slope of the exponential tail of SN 2004A roughly follows that of SN 1999em, who's rate of decay in the tail phase followed the decay of ^{56}Co (Elmhamdi et al. 2003b). The direct comparison to the light curve of SN 1987A assumes that SN 2004A deposited a similar fraction of γ-rays to SN 1987A. As the late-time decline of SN 1987A was also very close to the decay rate of ^{56}Co, this assumption is also not unfounded.

It is unfortunate that the light curve of SN 2004A was too sparse to obtain a reliable distance-independent result from the 'steepness' method. From the limits that were obtained using this method, the nickel mass is unlikely to be as low as $0.006\,M_\odot$. This is the same nickel mass, from Pastorello et al. (2004b) corrected to the revised distance of Hendry et al. (2005), as the low-nickel, low-luminosity ('faint') SN 1997D. SNe with low-nickel masses (e.g. Zampieri et al. 2003; Pastorello et al. 2004a,b) have low luminosities and velocities, hence have narrow features in their spectra. SN 2004A has none of these features and appears to be more similar to SN 1999em. The upper limit from the 'steepness of decline' method is consistent with the Hamuy (2003) and the direct comparison with SN 1987A methods. We therefore take the average of the former two methods to get $M_{\rm Ni} = 0.046^{+0.031}_{-0.017}$, where the error is the combined error of the methods.

6 ANALYSIS OF THE PROGENITOR IMAGES

6.1 Metallicity of NGC 6207 at the position of SN 2004

As can be seen in Fig. 1, the SN occurred at a significant distance from the centre of the galaxy NGC 6207. Given that the host galaxy is an Sc, with a likely strong abundance gradient (e.g. Vila-Costas & Edmunds 1992), it is possible that the environment was significantly metal poor and hence the progenitor star may have been of lower than solar metallicity. There is no measurement of the abundance gradient in NGC 6207, but as an illustrative argument we can estimate the likely metallicity at the galactic position of SN 2004A from the properties of NGC 6207. At a distance of 20.3±3.4 Mpc, NGC 6207 has $M_{\rm B} = -20.0 \pm 0.3$ from LEDA. Using the correlations between oxygen abundances and macroscopic galactic properties of Pilyugin, Vílchez & Contini (2004), NGC 6207 should have an oxygen abundance at $0.4R_{25}$ of $12 + \log {\rm O/H} \simeq 8.5 \pm 0.2$. Again using the parameters from LEDA, we find that $R_{25} = 4$ kpc and that SN 2004A lies at a galactocentric distance of $R_{\rm g} = 6.2$ kpc. The latter number assumes that SN 2004A occurred in the disc of NGC 6207 and is a deprojected distance assuming a disc inclination angle of 68.4° and a major axis angle of 17.5° (east of north). NGC 6207 appears to be an Sc galaxy, similar in morphology, size and absolute magnitude to M33 hence if we assume that the stellar oxygen abundance gradient in M33 (-0.05 dex kpc^{-1}; Urbaneja et al. 2005) is applicable in NGC 6207 then the oxygen abundance is likely to be 8.3 ± 0.4, where the error comes from a combination of the error estimate at $0.4R_{25}$ and the typical scatter in abundance gradients of Sc galaxies of ± 0.05 dex kpc^{-1}. Although the error is large, it suggests that the metallicity of the progenitor star was likely a factor of 2 below solar, similar to the Large Magellanic Cloud. The spectrum of SN 2004A does not show any distinct peculiarities compared to that of SN 1999em which likely arose from a RSG of approximately solar metallicity (Smartt et al. 2002). It would be of interest to determine the metallicity accurately in the region where SN 2004A exploded, from the nearest accessible H II regions.

6.2 Astrometry of *HST* observations

To determine the position of SN 2004A on the pre-explosion images, we employed the same differential method as in Smartt et al. (2004) and Maund & Smartt (2005). The position of SN 2004A was found to lie on the WF3 chip in all the pre-explosion observations made using WFPC2. The F606W and F814W pre-explosion observations were taken consecutively, and were found to be aligned to better than 0.01 arcsec. The positions of 16 stars, common to the pre-explosion WF3 F814W and post-explosion ACS F555W images, were measured using aperture photometry within the DAOPHOT package. The post-explosion F555W frame was transformed to the

WF3 pre-explosion coordinate system using the IRAF task GEOMAP. The F300W pre-explosion image, however, was taken ∼1 yr previously with a different telescope orientation, and a similar process was followed for alignment. Due to the pointing of the observation and the short wavelength band pass of the filter, only three stars could be identified on WF3 for use in the transformation calculation. It was possible to estimate an approximate position for the SN to roughly 0.14 arcsec, and since no objects are detected anywhere near the SN position the exact position is not critical.

The pixel location of SN 2004A was measured on the post-explosion frame, again using aperture photometry, and the same transformation was applied to this position to determine the coordinates of the SN in the pre-explosion images. In order to give an average value and estimated error, three different centring algorithms were employed to determine the SN centroid. Fig. 10 shows sections of the pre- and post-explosion imaging centred on the SN coordinates.

6.3 Detection of a progenitor star in F814W

There is no progenitor object visible in either the F606W or the F300W frames at the position of SN 2004A, however there is a faint object detected in the F814W frames. The object has a significance of 4.7σ measured with simple aperture photometry in a 2-pixel aperture. The PSF-fitting WFPC2 photometry package HSTPHOT (Dolphin 2000) also independently detects an object at 4.8σ, suggesting a star-like PSF. After aperture and CTE corrections, aperture photometry determined a flight system magnitude of $m_{\rm F814W} = 24.3 \pm 0.3$. The HSTPHOT magnitude was $m_{\rm F814W} = 24.4 \pm 0.2$, again after similar corrections. The astrometric errors and the difference in the position of the progenitor object and SN are listed in Table 13. The error in the position of the progenitor star in the undersampled WFPC2 image was estimated from the range of four methods used to determine the position, that is, three different centring algorithms within the aperture photometry routines of DAOPHOT and the PSF-fitting method within HSTPHOT. The error in the SN position was determined in a similar way. The geometric transformation error is a combination of the rms residuals from the two-dimensional spatial transformation functions. The total error of the differential astrometric solution is calculated by combining these three independent errors in quadrature. The difference in the position of the SN is 34 milliarcsec (mas), and the error in the method is 38 mas. Hence, within the errors, the progenitor object detected in the F814W image is coincident with the SN position.

It is therefore probable that this object is the progenitor star of SN 2004A. The agreement between the two different methods, the flux (and hence s/n), centroid, magnitude and error suggests that this is indeed a significant detection, with a magnitude of $m_{\rm F814W} = 24.35 \pm 0.3$. Fig. 10 shows that there are two hot pixels near the position of SN 2004A, which are clearly labelled in the associated data quality files released as part of the WFPC2 data package. However, there is no hot pixel flagged at the position of SN 2004A in the data quality files that would suggest a spurious detection. We have estimated 5σ limiting magnitudes for each of the filters, in the vicinity of the position of SN 2004A (i.e. using an appropriate local sky flux), and these are $m_{\rm F606W} = 25.4 \pm 0.3$, $m_{F814W} = 24.3 \pm 0.3$ and $m_{\rm F300W} = 23.1 \pm 0.3$. As expected, the 5σ limiting magnitude calculated for the F814W filter is consistent with the estimated magnitude of the 4.7σ object. In the discussion in Section 6.4, we argue that whether or not we interpret this as a real detection of the progenitor, or as an upper limit to the magnitude, the implications for the progenitor star are similar.

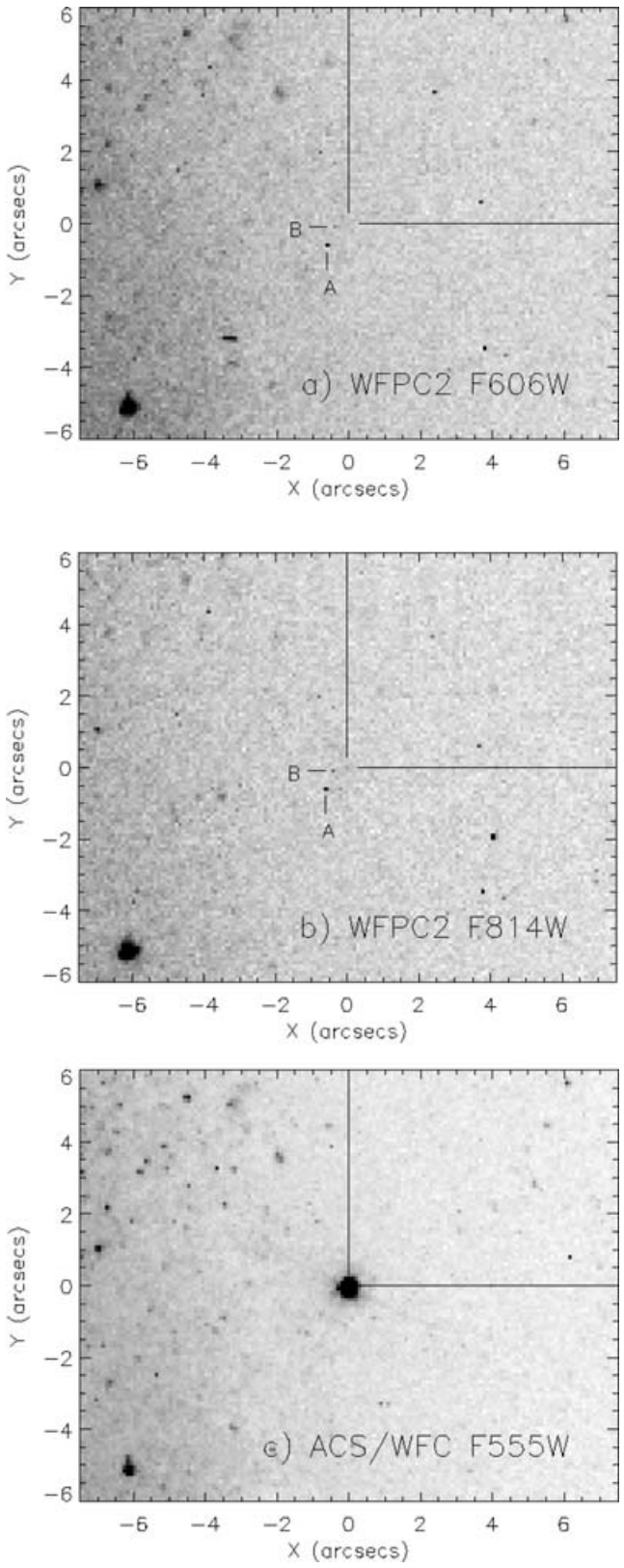

Figure 10. Pre- and post-explosion imaging of the site of SN 2004A. All images are centred on the SN location. (a) WFPC2 F606W pre-explosion image. (b) WFPC2 F814W pre-explosion image. The objects labelled A and B in these images are not stars but hot pixels. (c) ACS/WFC F555W post-explosion image. In the F814W pre-explosion image, a faint object is just visible at the SN location.

Table 13. Astrometric errors of the position of SN 2004A and the progenitor star detected in the F814W filter.

Source of Error	Error (mas)
Position of progenitor	11
Position of SN	10
Geometric transformation (rms)	35
Total error	38
Measured difference	34

6.4 Luminosity and mass limits for the progenitor of SN 2004A

First of all, we assume that the 4.7σ F814W object is a real detection of the progenitor star and combine this with the F606W limiting magnitude. The methods of Smartt et al. (2003) and Maund & Smartt (2005) were employed, in which the apparent flight system WFPC2 magnitudes are converted to bolometric luminosities appropriate for supergiant stars of a range of spectral types/effective temperatures.

The stellar evolutionary tracks used were the Geneva tracks (Schaller et al. 1992; Meynet et al. 1994) for single stars with initial masses ranging from 7 to 40 $M_\odot$ and solar metallicity ($Z = 0.02$). The issue of the metallicity was discussed in Section 6.1, and the evolutionary tracks of 8–12 $M_\odot$ stars are not particularly dependent on metallicity, unless extremely low values are reached, which is unlikely to be the case here. The limiting apparent magnitudes were converted first to absolute and then bolometric magnitudes. The distance to NGC 6207 was estimated as 20.3 ± 3.4 Mpc (see Section 4.3) and the foreground reddening in this direction is given as $E(B-V) = 0.015$, from NED. However, this does not of course take into account the reddening effects caused by the gas and dust of the star's host galaxy. The reddening toward the bright supergiants in the immediate vicinity of the SN from the three-colour ACS images was estimated as, $A_U = 0.29 \pm 0.15, A_V = 0.19 \pm 0.09$ and $A_I = 0.09 \pm 0.05$ in Section 3.2.

The apparent flight system magnitudes of the F814W and F606W observations were converted to standard *VI* filter magnitudes using the tabulated values in Maund & Smartt (2005). This correction is dependent on the spectral type of the object and hence extinction-corrected absolute magnitudes appropriate for supergiant stars of spectral types in the range of O9 to M5, ($T_{\rm eff}$ 32 000–2880 K) were calculated from the $m_{\rm F606W}$ and $m_{\rm F814W}$ flight system magnitudes. Smartt et al. (2001) have tabulated spectral type dependent corrections for $m_{\rm F300W}$ magnitudes, $c_{\rm V-300}$, which also include a colour correction to the standard V band, necessary for conversion to bolometric magnitudes. These absolute magnitudes were converted to bolometric magnitudes and luminosities (Table 14). The I-band luminosities with errors were plotted on a Hertzsprung–Russell (HR) diagram (Fig. 11), thereby defining a strip within which the object must be placed. To further constrain progenitor parameters, the V-band 5σ luminosity limit was also plotted, and possible progenitors must lie below this limit on the HR diagram. The I-band detection was thereby restricted to spectral types ranging from G5 to M5 ($T_{\rm eff} \sim 4900$ K to 2900 K), ruling out BSGs and suggesting that the progenitor of SN 2004A was a RSG just prior to explosion. The initial mass of the progenitor is estimated to be $9^{+3}_{-2}\,M_\odot$. The value of $9\,M_\odot$ comes from the closest estimated end point to the I-band magnitude, which is also consistent with the F606W limit. The upper error comes from the highest possible mass it is likely to have been, which is the highest mass track that the observed limits overlap in any significant way, and the lower limit is estimated in a similar way. This method was adopted in Smartt et al. (2004).

If the object detected in the F814W image is not a real detection, then the lines plotted on Fig. 11 can both be considered upper limits and the mass of $9^{+3}_{-2}\,M_\odot$, becomes a very robust upper mass limit of $<12\,M_\odot$. Hence, the important point to arise from this analysis is that the progenitor object can have had an initial mass of no more than $12\,M_\odot$, and was probably in the range $9^{+3}_{-2}\,M_\odot$.

Table 14. Luminosity limits on the progenitor of SN 2004A from the WFPC2 F300W (U), F606W (V) and F814W (I) pre-explosion observations. The luminosity values for the I band are estimated from the 4.7σ detection discussed above. The values for U and V are from the 5σ limiting magnitudes. The corrections for the F300W magnitudes were taken from Smartt et al. (2001). Corrections for F606W and F814W taken from Maund & Smartt (2005). The error on all values of $\log(L/L_\odot) = 0.2$.

Spectral type	$T_{\rm eff}$	$\log L/L_\odot$ (U)	$\log L/L_\odot$ (V)	$\log L/L_\odot$ (I)
O9	32000	–	5.73	6.27
B0	28500	5.99	–	–
B2	17600	5.45	5.06	5.53
B5	13600	5.53	4.79	5.23
B8	11100	5.76	4.67	5.08
A0	9980	–	4.56	4.96
A2	9380	–	4.51	4.89
A5	8610	–	4.43	4.79
F0	7460	6.04	4.37	4.68
F2	7030	–	4.36	4.65
F5	6370	–	4.36	4.62
F8	5750	–	4.37	4.59
G0	5370	6.30	4.38	4.57
G2	5190	–	4.39	4.53
G5	4930	–	4.42	4.53
G8	4700	–	4.45	4.55
K0	4550	6.80	4.48	4.55
K2	4310	–	4.50	4.51
K5	3990	–	4.59	4.40
M0	3620	7.52	4.70	4.48
M2	3370	7.64	4.83	4.50
M5	2880	8.38	5.44	4.49

7 DISCUSSION

7.1 What can we say about SN 2004A?

SN 2004A appears to be a 'normal' SN II-P with a spectrum and light curve very like the well-observed SN 1999em (Figs 4 and 5). The nickel mass found in Section 5 was also comparable to that of SN 1999em, as we would have expected. The existence of a low-luminosity, low-nickel mass, subgroup of SNe II-P (e.g. Zampieri et al. 2003; Pastorello et al. 2004a,b), has been suggested. One of the proposed characteristics of this group is a rapid excess in the $B-V$ and $V-R$ colours at the end of the photospheric phase (Pastorello et al. 2004b). Elmhamdi et al. (2003b) and Pastorello et al. (2004b) noted this rapid excess in the 'faint' SN 1997D (see Fig. 12), and it was also observed by Pastorello et al. (2004b) in SN 1999eu, another 'faint' SN, in the form of a sharp spike. Fig. 6 compares the colour evolutions of SN 2004A and SN 1999em. The $B-V$ colour evolution of SN 2004A clearly shows such a rapid excess at the end of the plateau, which is not seen in the colour curve

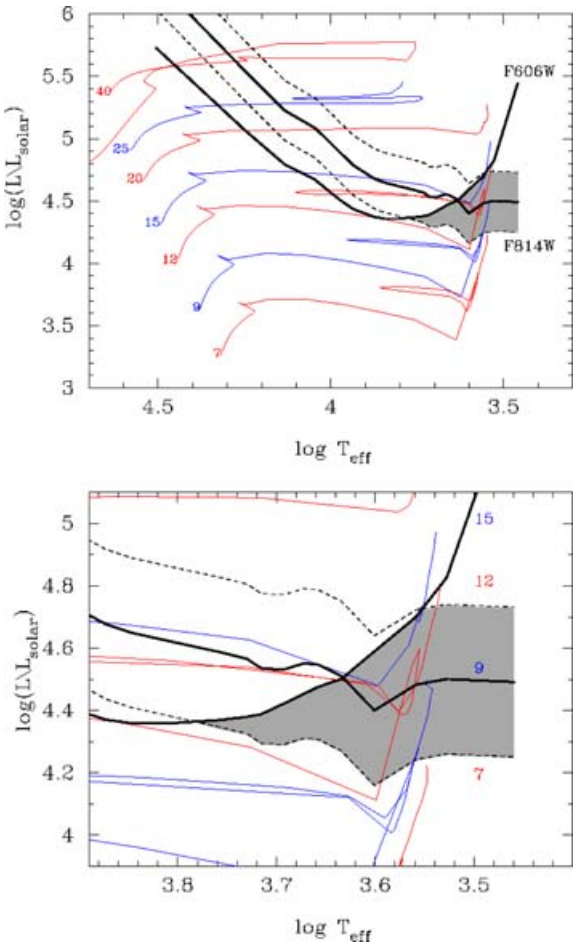

Figure 11. HR diagram showing the Geneva stellar evolutionary tracks (coloured red and blue alternatively for clarity, with initial masses labelled) and the likely position for the progenitor. The progenitor detected at 5σ in the I band has a luminosity dependent on effective temperature. This solid black curve, labelled F814W is plotted and bracketed by the likely errors (dotted curve, see text). The solid black curve labelled F606W is the limiting luminosity implied by the sensitivity of the F606W pre-explosion images. All stars lying above this line would have been detectable in the diagram. Hence combining these two constraints suggests a region of possible existence for progenitor stars. This region is shaded grey, and implies the progenitor was likely a RSGs with initial masses of 9^{+3}_{-2} M$_{\odot}$. The lower panel is a magnified view of the interesting shaded region shown in the upper panel.

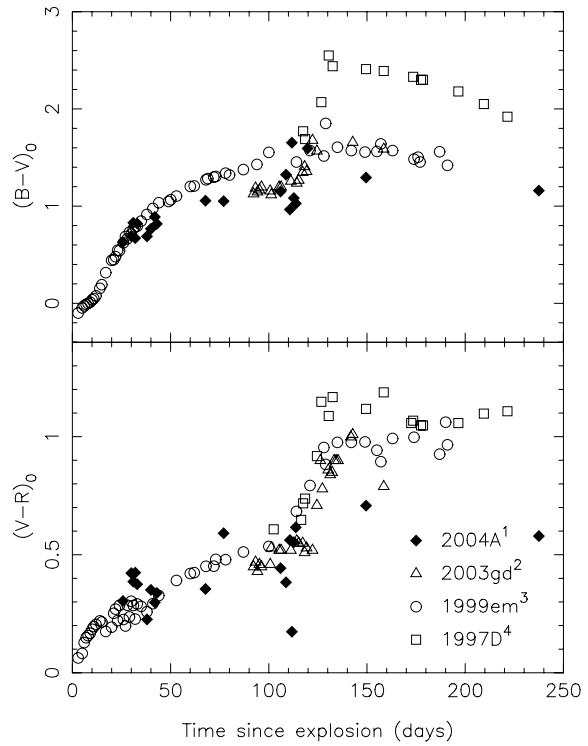

Figure 12. Intrinsic $B-V$ and $V-R$ colour curves of SN 2004A alongside those of the prototypical peculiar 'faint' SN 1997D, the 'normal' SNe 1999em and 2003gd. The superscripts in the figure denote the source of the photometry: (1) this paper, (2) Hendry et al. (2005), (3) Hamuy et al. (2001) and (4) Benetti et al. (2001).

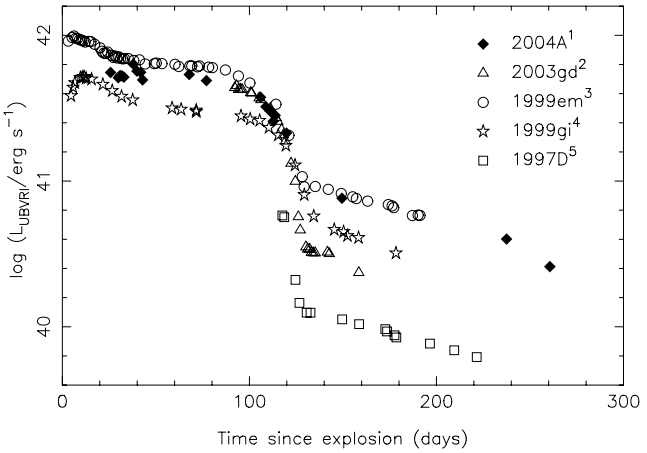

Figure 13. Comparison between the UVOIR light curves of SNe 2004A, 2003gd, 1999em, 1999gi and 1997D which have nickel masses of 0.046, 0.016, 0.048, 0.022 and 0.006 M$_{\odot}$, respectively. The nickel mass for all the SNe, apart from SN 2004A which is given in this paper, are from Hendry et al. (2005), and references therein. The superscripts in the figure denote the source of the photometry: (1) this paper, (2) Hendry et al. (2005), (3) Hamuy et al. (2001), (4) Leonard et al. (2002) and (5) Benetti et al. (2001).

of SN 1999em. Fig. 12 shows a comparison of the colour curves of the prototypical peculiar 'faint' SN 1997D (Benetti et al. 2001), and the 'normal' SNe 1999em and 2003gd (Hamuy et al. 2001; Hendry et al. 2005). Although the excess is present in the $B-V$ colour curve of SN 2004A, it does not show as great an excess as SN 1997D, but instead follows a similar curve to SN 2003gd with a slightly bluer tail. There is too large a scatter in the $V-R$ colour curve to be of much use, but there does not appear to be any evidence of a colour excess. The appearance of the spectrum and the light curves imply that SN 2004A is a normal SN II-P, suggesting that this excess is not confined to the ranks of the 'faint' SNe. Until we have a larger sample of SNe II-P, both 'faint' and 'normal', it is difficult to confirm or rule out this as a characteristic.

A comparison between the UVOIR light curves of SNe 2004A, 2003gd, 1999em, 1999gi and 1997D is shown in Fig. 13. All the UVOIR light curves, apart from SN 2004A, are from Hendry et al. (2005) and a full description of how they were constructed can be found there. The UVOIR light curve of SN 2004A, which was constructed in the same way, also confirms the similarities between SN 2004A and the other normal SNe II-P. SN 2004A differs slightly from SN 1999em in the plateau with SN 2004A being marginally

fainter, whereas the tail luminosities reflect the comparable nickel mass ejected.

7.2 Implications for the progenitor of SN 2004A

We compared the observed properties of SN 2004A with the progenitor mass, presented in Section 6, using equation (2) of Litvinova & Nadyozhin (1985). The equations of Litvinova & Nadyozhin relate the explosion energy, mass of the envelope expelled ($M_{\rm ej}$) and initial radius of the star just before the explosion, to the observed quantities of SNe. Nadyozhin (2003) used a sample of 14 SNe to test these equations and found that they gave reasonable results. Equation (2) of Litvinova & Nadyozhin (1985), is shown here in equation (7), where $M_{\rm ej}$ is the ejected envelope mass, Δt is the length of the plateau and $u_{\rm ph}$ is the velocity of the photosphere material in the middle of the plateau.

$$\log\left(\frac{M_{\rm ej}}{\rm M_\odot}\right) = 0.234M_V + 2.91\log\left(\frac{\Delta t}{\rm d}\right) + 1.96\log\left(\frac{u_{\rm ph}}{10^3\ {\rm km\ s^{-1}}}\right) - 1.829 \quad (7)$$

If we consider the UVOIR light curve in Fig. 13, the length of the plateau is ∼80 d, although it is difficult to be confident as the SN was not observed close to explosion. We therefore estimate the length of the plateau to be $\Delta t = 80^{+25}_{-5}$ d, where the positive error is very conservative. Using the reddening estimated in Section 3.2, the parameters discussed in Section 4.1 for the SCM at 50-d post explosion and the distance estimated in Section 4.3, we found that the ejecta mass was $M_{\rm ej} = 11^{+10}_{-4}$. If we assume that the compact remnant plus other mass losses from the system is $2 \pm 1\,{\rm M_\odot}$ then it suggests that $M_{\rm MS} = 13^{+10}_{-4}\,{\rm M_\odot}$ for SN 2004A, where the upper mass limit of $23\,{\rm M_\odot}$ is a hard upper limit as the error in the plateau is very conservative. The lower limit of this is consistent with the progenitor mass, $9^{+3}_{-2}\,{\rm M_\odot}$, found from pre-explosion images in Section 6. This result may also suggest that equation (7) overestimates the mass somewhat as the lower limit is only just consistent even though our lower limits are fairly well constrained.

The observations of progenitors do not only have important implications for stellar evolution theory, but also for the progenitor models of 'faint' SNe II-P. There are two very different plausible models for these, one being the low-energy explosion of massive stars (e.g. Turatto et al. 1998; Benetti et al. 2001; Zampieri et al. 2003). In this model, the collapsing core forms a black hole and a significant amount of fallback of material occurs. An alternative scenario is the low-energy explosion of low-mass stars, presented by Chugai & Utrobin (2000) who successfully reproduced the observations of SN 1997D with an explosion of 10^{50} ergs and an ejected mass of $6\,{\rm M_\odot}$. The findings of Zampieri, Ramina & Pastorello (2004) support the high-mass progenitor scenario. The authors find a bimodal distribution of SNe in the nickel mass, $M_{\rm MS}$ plane. A reproduction of the authors' Fig. 1 (right) is shown here in Fig. 14. We are beginning to populate this figure with direct measurements of the main-sequence mass of the progenitors, as opposed to model-dependent values. The most interesting feature of this figure, and the most controversial, is the existence of the faint branch. The SNe which populate this branch are proposed to have high initial mass progenitors. The points with direct measurements, or robust limits, of progenitor mass from pre-explosion imaging are highlighted with the filled circles. This figure, however, should be treated with caution as the theoretical estimates of $M_{\rm MS}$ from Zampieri et al. (2004), shown with open circles in the figure, will most probably need to be revised using the value of the opacity from Hendry et al. (2005). The observed nickel masses are estimated from the light curves, and are from Hamuy (2003) for SN 1999br and from Hendry et al. (2005, and references therein) for SNe 2003gd and 1999em. The Zampieri et al. nickel masses are, however, an input parameter of the semi-analytical light curve code and are therefore theoretical. $M_{\rm MS}$ for SN 2003gd is from Smartt et al. (2004), whereas SNe 1999em and 1999br are upper mass limits only and are from Smartt et al. (2002) and Maund & Smartt (2005), respectively. SN 2004A comfortably sits in the 'normal' branch of the bimodal distribution. Even though the mass limit of SN 1999br rules out a high-mass progenitor for this 'faint' SN, it does not necessarily rule out a high-mass progenitor scenario for other 'faint' SNe. It does, however, suggest that for at least some 'faint' SNe a low-mass progenitor is likely. With more upper mass limits or direct detections of the progenitor stars of these SNe, we should be able to determine the validity of the high-mass progenitor scenario.

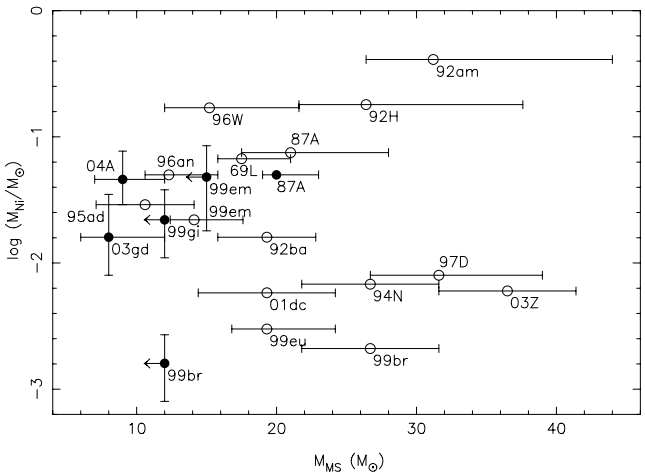

Figure 14. Reproduction of fig. 1 (right) of Zampieri et al. (2004) showing the bimodal distribution of SNe II-P, in the $M_{\rm Ni}/M_{\rm MS}$ plane, from their model. The open circles show theoretical data from the semi-empirical model of Zampieri et al. (2003), where $M_{\rm MS}$ is estimated from the ejected envelope mass. The filled circles show observational data for SNe 2004A, 2003gd, 1999em and 1999br, where the observed nickel masses are estimated from the light curve. The nickel masses for SNe 2003gd and 1999em are from Hendry et al. (2005) and SN 1999br is from Hamuy (2003). $M_{\rm MS}$ for SNe 1999em and 1999br are upper mass limits only and are from Smartt et al. (2002) and Maund & Smartt (2005), respectively. SN 2004A comfortably sits in the in the 'normal' branch of the bimodal distribution.

8 CONCLUSION

We presented photometric and spectroscopic data of the Type II-P SN 2004A, comparing the *BVRI* light curves with those of the well-observed SN 1999em using a χ^2-fitting algorithm. This analysis allowed us to estimate an explosion epoch of JD $245\,3011^{+3}_{-10}$, corresponding to a date of 2004 January 6. We estimated the extinction of the SN as $E(B-V) = 0.06 \pm 0.03$, using *HST* ACS photometry of the neighbouring stars and confirmed the reddening using the SN's colour evolution. The expansion velocity was measured from our only spectrum, and was found to be comparable to the velocities of similar SNe II-P. This enabled us to extrapolate the velocity evolution of SN 2004A forwards 7 d to find the velocity at a phase of 50 d, to be used in the SCM distance estimate.

Three new distances to NGC 6207 were calculated using two different methods, the SCM (Hamuy 2003, 2004a,b) and the BSM

(Rozanski & Rowan-Robinson 1994; Karachentsev & Tikhonov 1994). First, using the extrapolated velocity and interpolated *VI* magnitudes, we estimated a distance of $D = 21.0 \pm 4.3$ Mpc with the SCM. We then used *HST* (ACS HRC) photometry to estimate the distances of 21.4 ± 3.5 and 25.1 ± 1.7 Mpc using two different BSM calibrations. Using these three distances and other distances within the literature, we estimated an overall distance of 20.3 ± 3.4 Mpc to NGC 6207. This distance allowed the nickel mass synthesized in the explosion to be estimated, $M_{\rm Ni} = 0.046^{+0.031}_{-0.017}\,{\rm M}_{\odot}$, comparable to that of SN 1999em.

The probable discovery of the progenitor of SN 2004A on pre-explosion *HST* WFPC2 images was presented. The star that exploded was likely to have been a RSG with a mass of $9^{+3}_{-2}\,{\rm M}_{\odot}$. If the 4.8σ detection is not believed then the 5σ upper limit in the F814W images implies a robust upper mass limit for a RSG progenitor of $12\,{\rm M}_{\odot}$. This is only the seventh progenitor star of an unambiguous core-collapse SN that has had a direct detection. The first two progenitors discovered were those of SN 1987A, which was a BSG, and SN 1993J, which arose in a massive interacting binary system. Neither of these fitted in with the theory that RSGs explode to give Type II SNe. However, it appears that the elusive RSG progenitors are now being found, with the discovery of the progenitor of SN 2004A being the third (after SNe 2003gd and 2005cs).

The observations of SN 2004A were compared to those of other SNe II-P and were found to be consistent with other normal SNe II-P, although there is a small peak in the UVOIR light curve at around 40 d, which could just be an artifact of the photometry. The SN observations were then compared to the mass of the progenitor using theoretical relationships which relate the mass of the envelope expelled to the observed quantities of SNe, and were found also to be consistent. We conclude that SN 2004A was a normal Type II-P SNe that arose from the core-collapse induced explosion of a red supergiant of mass $9^{+3}_{-2}\,{\rm M}_{\odot}$.

ACKNOWLEDGMENTS

Based on observations made with the NASA/ESA *Hubble Space Telescope*, obtained from the data archive at the Space Telescope Science Institute. STScI is operated by the Association of Universities for Research in Astronomy, Inc., under NASA contract NAS 5-26555. The spectroscopic data presented were obtained at the W.M. Keck Observatory, which is operated as a scientific partnership among the California Institute of Technology, the University of California and the National Aeronautics and Space Administration. The Observatory was made possible by the generous financial support of the W.M. Keck Foundation. The authors wish to recognize and acknowledge the very significant cultural role and reverence that the summit of Mauna Kea has always had within the indigenous Hawaiian community. We are most fortunate to have the opportunity to conduct observations from this mountain. Some data presented were taken with the Liverpool Telescope at the Observatorio del Roque de Los Muchachos, La Palma Spain. The authors would like to express their thanks to the research staff at Caltech and Palomar Observatory who made the P60 automation possible. The initial phase of the P60 automation project was funded by a grant from the Caltech Endowment, with additional support for this work provided by the NSF and NASA. AGY acknowledges support by NASA through Hubble Fellowship grant #HST-HF-01158.01-A awarded by STScI, which is operated by AURA, Inc., for NASA, under contract NAS 5-26555. SJS acknowledges funding from PPARC and the European Science Foundation in the forms of Advanced and EURYI fellowships. MAH thanks PPARC and Queen's University, Belfast for their financial support.

REFERENCES

Aldering G., Humphreys R. M., Richmond M., 1994, AJ, 107, 662
Bahcall J. N., Soneira R. M., 1981, ApJS, 47, 357
Baron E., Cooperstein J., Kahana S., 1985, Phys. Rev. Lett., 55, 126
Baron E. et al., 2000, ApJ, 545, 444
Benetti S. et al., 2001, MNRAS, 322, 361
Cardelli J. A., Clayton G. C., Mathis J. S., 1989, ApJ, 345, 245
Chevalier R. A., 1976, ApJ, 207, 872
Chugai N. N., Utrobin V. P., 2000, A&A, 354, 557
Dolphin A. E., 2000, PASP, 112, 1383
Drilling J. S., Landolt A. U., 2000, in Arthur N. Cox, ed., Allen's Astrophysical Quantities, 4th edn. AIP Press, Springer, New York, ISBN: 0387987460
Eastman R. G., Schmidt B. P., Kirshner R., 1996, ApJ, 466, 911
Eldridge J. J., Tout C. A., 2004, MNRAS, 353, 87
Elmhamdi A., Chugai N. N., Danziger I. J., 2003a, A&A, 404, 1077
Elmhamdi A. et al., 2003b, MNRAS, 338, 939
Freedman W. L. et al., 2001, ApJ, 553, 47
Gal-Yam A., Cenko S. B., Fox D. W., Leonard D. C., Moon D.-S., Sand D. J., Soderberg A. M., 2004, Am. Astron. Soc. Meet. Abs., 205 #40.06
Gal-Yam A. et al., 2005, ApJ, 630, L29
Hamuy M., 2001, PhD thesis Univ. Arizona
Hamuy M., 2003, ApJ, 582, 905
Hamuy M., 2004a, in Freedman W. L., ed., Measuring and Modeling the Universe, Carnegie Observatories Astrophysics Series, preprint (astro-ph/0301281)
Hamuy M., 2004b, in Marcaide J. M., Weiler K. W., eds, Cosmic Explosions. On the 10th Anniversary of SN 1993J, IAU Colloquium 192. Springer, Heidelberg, p. 535
Hamuy M., Pinto P. A., 2002, ApJ, 566, L63
Hamuy M. et al., 2001, ApJ, 558, 615
Heger A., Fryer C. L., Woosley S. E., Langer N., Hartmann D. H., 2003, ApJ, 591, 288
Hendry M. A. et al., 2005, MNRAS, 359, 906
Howarth I. D., Murray J., Mills D., Berry D. S., 2003, Starlink User Note 50.24. Rutherford Appleton Laboratory
Karachentsev I. D., Tikhonov N. A., 1994, A&A, 286, 718
Kawakita H., Kinugasa K., Ayani K., Yamaoka H., 2004, IAUC, 8266, 2
Leonard D. C., Kanbur S. M., Ngeow C. C., Tanvir N. R., 2003, ApJ, 594, 247
Leonard D. C. et al., 2002, PASP, 114, 35
Leonard D. C. et al., 2002, AJ, 124, 2490
Li W., Van Dyk S. D., Filippenko A. V., Cuillandre J., 2005, PASP, 117, 121
Li W., Van Dyk S. D., Filippenko A. V., Cuillandre J., Jha S., Bloom J. S., Riess A. G., Livio M., 2006, ApJ, 641, 1060
Litvinova I. Y., Nadyozhin D. K., 1985, SvAL, 11, 145
Maíz-Apellániz J., Bond H. E., Siegel M. H., Lipkin Y., Maoz D., Ofek E. O., Poznanski D., 2004, ApJ, 615, L113
Mathis J. S., 2000, in Cox A. N., ed., Allen's Astrophysical Quantities, 4th edn. Springer, New York, p. 523
Maund J. R., 2005, PhD thesis, Univ. of Cambridge
Maund J. R., Smartt S. J., 2005, MNRAS, 360, 288
Maund J. R., Smartt S. J., Danziger I. J., 2005, MNRAS, L88
Maund J. R., Smartt S. J., Kudritzki R. P., Podsiadlowski P., Gilmore G. F., 2004, Nat, 427, 129
Meynet G., Maeder A., Schaller G., Schaerer D., Charbonnel C., 1994, A&AS, 103, 97
Nadyozhin D. K., 2003, MNRAS, 346, 97
Nakano S., Itagaki K., Kushida R., Kushida Y., 2004, IAUC, 8265, 1
Pastorello A., Ramina M., Zampieri L., Navasardyan H., Salvo M., Fiaschi M., 2004a, in Marcaide J. M., Weiler K. W., eds, Cosmic Explosions. On the 10th Anniversary of SN 1993J, IAU Colloquium 192. Springer, Heidelberg, p. 195

Pastorello A. et al., 2004b, MNRAS, 347, 74
Pilyugin L. S., Vílchez J. M., Contini T., 2004, A&A, 425, 849
Rajala A. M. et al., 2005, PASP, 117, 132
Rozanski R., Rowan-Robinson M., 1994, MNRAS, 271, 530
Schaller G., Schaerer D., Meynet G., Maeder A., 1992, A&AS, 96, 269
Schlegel D. J., Finkbeiner D. P., Davis M., 1998, ApJ, 500, 525
Smartt S. J., Gilmore G. F., Tout C. A., Hodgkin S. T., 2002, ApJ, 565, 1089
Smartt S. J., Gilmore G. F., Trentham N., Tout C. A., Frayn C. M., 2001, ApJ, 556, L29
Smartt S. J., Maund J. R., Gilmore G. F., Tout C. A., Kilkenny D., Benetti S., 2003, MNRAS, 343, 735
Smartt S. J., Maund J. R., Hendry M. A., Tout C. A., Gilmore G. F., Mattila S., Benn C. R., 2004, Sci, 303, 499
Sohn Y., Davidge T. J., 1996, AJ, 111, 2280
Theureau G., Bottinelli L., Coudreau-Durand N., Gouguenheim L., Hallet N., Loulergue M., Paturel G., Teerikorpi P., 1998, A&AS, 130, 333
Tonry J. L., Blakeslee J. P., Ajhar E. A., Dressler A., 2000, ApJ, 530, 625
Tully R. B., 1988, Nearby Galaxies Catalog. Cambridge Univ. Press, Cambridge and New York, p. 221
Tully R. B., Shaya E. J., 1984, ApJ, 281, 31
Turatto M. et al., 1998, ApJ, 498, L129
Urbaneja M. A., Herrero A., Kudritzki R.-P., Najarro F., Smartt S. J., Puls J., Lennon D. J., Corral L. J., 2005, ApJ, 635, 311
Van Dyk S. D., Garnavich P. M., Filippenko A. V., Höflich P., Kirshner R. P., Kurucz R. L., Challis P., 2002, PASP, 114, 1322
Van Dyk S. D., Li W., Filippenko A. V., 2003a, PASP, 115, 1
Van Dyk S. D., Li W., Filippenko A. V., 2003b, PASP, 115, 1289
Vila-Costas M. B., Edmunds M. G., 1992, MNRAS, 259, 121
Walborn N. R., Prevot M. L., Prevot L., Wamsteker W., Gonzalez R., Gilmozzi R., Fitzpatrick E. L., 1989, A&A, 219, 229
White G. L., Malin D. F., 1987, Nat, 327, 36
Zampieri L., Pastorello A., Turatto M., Cappellaro E., Benetti S., Altavilla G., Mazzali P., Hamuy M., 2003, MNRAS, 338, 711
Zampieri L., Ramina M., Pastorello A., 2004, in Marcaide J. M., Weiler K. W., eds, IAU Colloq. 192, Cosmic Explosions. On the 10th Anniversary of SN 1993J. Springer, Heidelberg, p. 275

This paper has been typeset from a TEX/LATEX file prepared by the author.